

Fermion Generations and Mixing from Dualized Standard Model ¹

CHAN Hong-Mo

h.m.chan@rl.ac.uk

*Rutherford Appleton Laboratory,
Chilton, Didcot, Oxon, OX11 0QX, United Kingdom*

TSOU Sheung Tsun

tsou@maths.ox.ac.uk

*Mathematical Institute, University of Oxford,
24-29 St. Giles', Oxford, OX1 3LB, United Kingdom*

Abstract

The puzzle of fermion generations is generally recognized as one of the most outstanding problems of present particle physics. In these lectures, we review a possible solution based on a nonabelian generalization of electric–magnetic duality derived some years ago. This nonabelian duality implies the existence of another $SU(3)$ symmetry dual to colour, which is necessarily broken when colour is confined and so can play the role of the “horizontal” symmetry for fermion generations. When thus identified, dual colour then predicts 3 and only 3 fermion generations, besides suggesting a special Higgs mechanism for breaking the generation symmetry. A phenomenological model with a Higgs potential and a Yukawa coupling constructed on these premises is shown to explain immediately all the salient qualitative features of the fermion mass hierarchy and mixing pattern, excepting for the moment CP-violation. In particular, though treated on exactly the same footing, quarks and leptons are seen to have very different mixing patterns as experimentally observed, with leptons having generally larger mixings than quarks. The model offers further a perturbative method for calculating mixing parameters and mass ratios between generations. Calculations already carried out to 1-loop order is shown to give with only 3 adjustable parameters the following quantities all to within present experimental error: all 9 CKM matrix elements $|V_{rs}|$ for

¹Course of lectures given at the 42nd Cracow School of Theoretical Physics, 2002.

quarks, the neutrino oscillation angles or the MNS lepton mixing matrix elements $|U_{\mu 3}|, |U_{e 3}|$, and the mass ratios $m_c/m_t, m_s/m_b, m_\mu/m_\tau$. The special feature of this model crucial for deriving the above results is a fermion mass matrix which changes its orientation (rotates) in generation space with changing energy scale, a feature which is shown to have direct empirical support, and although potentially dangerous for flavour-violation is found through detailed analysis not to be the case. With its parameters now so fitted, the resulting scheme is highly predictive giving in particular correlated predictions in low energy FCNC effects (meson mass splittings and decays, $\mu - e$ conversion in nuclei, etc.) and in ultra-high energy (post-GZK) air showers from cosmic rays, both of which can hopefully be tested soon by experiment.

1 Introduction

As far as we know today, quarks and leptons, the fermionic fundamental building blocks of our material world, each occurs in 3, and apparently only 3, copies called generations having very similar properties apart from their masses. The masses, however, vary greatly, dropping from generation to generation by about one to more than two orders of magnitude depending on the fermion species. For charged leptons and quarks, the masses are now quite well determined and are listed in the Particle Physics Booklet [1] as follows:

$$\begin{aligned} m_t &\sim 175 \text{ GeV}, & m_c &\sim 1.2 \text{ GeV}, & m_u &\sim 3 \text{ MeV}; \\ m_b &\sim 4.2 \text{ GeV}, & m_s &\sim 120 \text{ MeV}, & m_d &\sim 6 \text{ MeV}; \\ m_\tau &= 1.777 \text{ GeV}, & m_\mu &= 105.6 \text{ MeV}, & m_e &= 0.51 \text{ MeV}. \end{aligned} \tag{1.1}$$

For neutrinos, the picture is not yet as clear, but with the recent discovery of ν_τ , and observation of neutrino oscillations with measurement of some of the relevant parameters, a similar pattern looks increasingly likely to emerge, namely again 3 generations of neutrinos with a hierarchical mass spectrum.

That this should be the case has long been regarded theoretically as quite a mystery. First of all, that nature should want several species of fermions with different quantum numbers and interactions to build her multifarious world seems understandable, but why 3 copies of each? And, what is more, why has she given them so different masses? Indeed, the general theoretical idea is that particles get their masses mostly from self-energy through their interactions. Why then these widely different masses for the 3 generations which have as far as we know identical interactions? In fact, long before the full picture is known, the existence of the muon has already prompted Feynman to post above his bed the famous question: “Why does the muon weigh?” And now, with 3 generations in each of all 4 fermion species, and each generation weighing more than the next by large factors, Feynman’s question has become even more pressing.

And the mystery does not end there. With more empirical information accumulated, another puzzling phenomenon soon revealed itself. The 12 fermion states of different generations and species can each be represented by a state vector in 3-dimensional generation space. Within each species, the 3 generations are independent quantum states and should thus be represented by orthogonal vectors forming together an orthonormal triad. For quarks, for example, the 3 up quark states t, c, u form together a U triad, while the 3 down quark states b, s, d form together a D triad. The question, first posed

by Cabbibo [2], then arises, namely whether the U and D triads are the same, and if not, how they are related. Now the relative orientations, namely the inner (or dot) products, between any pairs of vectors in the 2 triads can be inferred empirically from experiment on e.g. hadron decays. The matrix of these inner products is then the famous CKM matrix [2, 3], for which the latest empirical information is summarized in [1] as follows:

$$\begin{pmatrix} |V_{ud}| & |V_{us}| & |V_{ub}| \\ |V_{cd}| & |V_{cs}| & |V_{cb}| \\ |V_{td}| & |V_{ts}| & |V_{tb}| \end{pmatrix} = \begin{pmatrix} 0.9742 - 0.9757 & 0.219 - 0.226 & 0.002 - 0.005 \\ 0.219 - 0.225 & 0.9734 - 0.9749 & 0.037 - 0.043 \\ 0.004 - 0.014 & 0.035 - 0.043 & 0.9990 - 0.9993 \end{pmatrix}. \quad (1.2)$$

One notices that the U and D triads are indeed not aligned but are nevertheless tantalisingly close to being so, namely that the CKM matrix is close to being the unit matrix. One notices also that the off-diagonal (mixing) elements seem to have hierarchical values with $|V_{us}|, |V_{cd}| \gg |V_{cb}|, |V_{ts}| \gg |V_{ub}|, |V_{ts}|$.

The same question can be repeated for leptons, i.e. on the relative orientation between the up and down triads, namely between the triad L of the charged leptons τ, μ, e and the triad N of the neutrino mass eigenstates traditionally denoted in order of decreasing mass by ν_3, ν_2, ν_1 . The matrix of inner products between pairs of vectors, one from each triad, is in this case known as the MNS matrix [4], the elements of which are measured in neutrino oscillation experiments. So far, experiments on atmospheric neutrinos from μ decay [5, 6] have shown that the mixing between the muon neutrino and the heaviest mass eigenstate ν_3 , namely the MNS element $U_{\mu 3}$, is near maximal. Those on solar neutrinos [5, 7, 8, 9, 10] measure the mixing between the electron neutrino and the second heaviest mass eigenstate ν_2 , namely the MNS element $U_{e 2}$, while reactor experiments such as CHOOZ [11] have given bounds on the mixing between the electron neutrino and ν_3 , namely the MNS element $U_{e 3}$. The total empirical information on the MNS matrix available to-date is briefly summarized below:

$$\begin{pmatrix} |U_{e1}| & |U_{e2}| & |U_{e3}| \\ |U_{\mu 1}| & |U_{\mu 2}| & |U_{\mu 3}| \\ |U_{\tau 1}| & |U_{\tau 2}| & |U_{\tau 3}| \end{pmatrix} = \begin{pmatrix} \star & 0.4 - 0.7 & 0.0 - 0.15 \\ \star & \star & 0.56 - 0.83 \\ \star & \star & \star \end{pmatrix}. \quad (1.3)$$

There are actually several solutions to the solar neutrino problem still consistent with present experiment, among which the so-called large mixing angle

MSW [12] solution is the most favoured and is the one quoted in (1.3). One notices that in contrast to the CKM matrix, the MNS matrix is far from diagonal, with some off-diagonal elements very large, but still the corner element U_{e3} is much smaller than the other two.

Thus, together with the markedly hierarchical mass spectra, the mixing patterns of quarks and leptons constitute a vast amount of quantitative data needing theoretical understanding. In spite of its many successes, however, the Standard Model as conventionally formulated offers no explanation at all either for the existence of the 3 fermion generations in the first place, nor yet for their striking mass and mixing patterns, but takes instead all these features just as fundamental inputs. Indeed, fermion masses and mixings together account for some three quarters of the twenty odd parameters defining the Standard Model, which would be dramatically reduced if some understanding of the generation puzzle can somehow be achieved. For this reason, the solution of the generation puzzle is justly regarded by many as one of the most urgent problems facing particle physics today.

In these lectures, we wish to describe a possible solution to the problem based on a nonabelian generalization of electric–magnetic duality. It is a solution within the Standard Model framework, without introducing, for example, either supersymmetry or higher dimensions, although it is not, as far as is known, inconsistent with either of these extensions. Apart from offering right from the start a *raison d’être* for 3 generations of fermions, this scheme, which we call the Dualized Standard Model (DSM), explains the fermion mass hierarchy and the mixing phenomena and suggests even a perturbative method for calculating mass and mixing parameters. Calculations with it have been carried out so far to the 1-loop level, and the score to-date is as follows. With 3 real parameters fitted to data, it gives correctly to within present experimental bounds the following measured quantities: the mass ratios $m_c/m_t, m_s/m_b, m_\mu/m_\tau$, all 9 elements $|V_{rs}|$ of the CKM matrix, plus the 2 elements $|U_{\mu 3}|$ and $|U_{e 3}|$ of the MNS matrix measured in neutrino oscillation experiments. It gives further by interpolation sensible though inaccurate estimates for the following quantities which are formally beyond the scope of the 1-loop calculation so far performed: the mass ratios $m_u/m_t, m_d/m_b, m_e/m_\tau$ and the solar neutrino angle U_{e2} . These calculated and estimated quantities represent altogether 12 independent fundamental parameters of the Standard Model, which are thereby replaced by only 3 fitted parameters in the DSM. Next, with nearly all its parameters now fixed, the scheme becomes highly predictive. In particular, numerous detailed predictions have been made in flavour-violation effects over a wide area comprising meson mass differences,

rare hadron decays, e^+e^- collisions, and muon–electron conversion in nuclei. Further predictions have been made on effects as far apart in energy as neutrinoless double-beta decays in nuclei and cosmic ray air showers beyond the GZK cut-off of 10^{20} eV at the extreme end of the present observable energy range. Wherever possible, these predictions have been confronted with data, and so far, all are found to remain within present empirical bounds, although a few of them so closely as should be accessible soon to new experimental tests.

Of course, that the DSM scheme seems to have largely succeeded in its primary aim of explaining fermion generations and their mass and mixing patterns, and at the same time to have survived all other tests to-date, still does not mean that its tenets are thereby proved correct. Stress should thus be given to examining the result to see which of its basic assumptions are really essential for obtaining the claimed agreement with experiment. At the same time, attention has to be paid to any aspects in the scheme which can potentially be improved. We hope to cover most of these topics, though some only briefly, in the course of these lectures.

2 Electric–magnetic duality and its nonabelian generalization

Let us start, however, from the beginning, with a reminder of ordinary electric–magnetic duality and a review of its extension to nonabelian Yang–Mills theory, then see eventually how it leads one to consider the Dualized Standard Model for an explanation of fermion generations. For the reader interested mainly in the phenomenological aspects of DSM and not so much in its theoretical basis, only a cursory look at this section is needed, since no mastery of the details contained in here is required for appreciation of the material in the later sections.

The Maxwell equations for electromagnetism are usually written as:

$$\left. \begin{array}{l} \operatorname{div} \mathbf{E} = \rho \\ \operatorname{curl} \mathbf{B} - \partial \mathbf{E} / \partial t = \mathbf{J} \end{array} \right\} \partial_\nu F^{\mu\nu} = -j^\mu$$

$$\left. \begin{array}{l} \operatorname{div} \mathbf{B} = 0 \\ \operatorname{curl} \mathbf{E} + \partial \mathbf{B} / \partial t = 0 \end{array} \right\} \partial_\nu {}^*F^{\mu\nu} = 0,$$
(2.1)

where the *dual field tensor* $*F^{\mu\nu}$ is defined to be

$$*F^{\mu\nu} = -\frac{1}{2}\epsilon^{\mu\nu\rho\sigma} F_{\rho\sigma}. \quad (2.2)$$

We see immediately that in the absence of matter, classical Maxwell theory is invariant under duality:

$$\partial_\nu *F^{\mu\nu} = 0 \quad [dF = 0] \quad (2.3)$$

$$\partial_\nu F^{\mu\nu} = 0 \quad [d*F = 0] \quad (2.4)$$

where in square brackets are displayed the equivalent equations in the language of differential forms. Then by the Poincaré lemma we deduce directly the existence of potentials A and \tilde{A} such that

$$F_{\mu\nu}(x) = \partial_\nu A_\mu(x) - \partial_\mu A_\nu(x) \quad [F = dA], \quad (2.5)$$

$$*F_{\mu\nu}(x) = \partial_\nu \tilde{A}_\mu(x) - \partial_\mu \tilde{A}_\nu(x) \quad [*F = d\tilde{A}]. \quad (2.6)$$

The two potentials transform independently under independent gauge transformations Λ and $\tilde{\Lambda}$:

$$A_\mu(x) \mapsto A_\mu(x) + \partial_\mu \Lambda(x), \quad (2.7)$$

$$\tilde{A}_\mu(x) \mapsto \tilde{A}_\mu(x) + \partial_\mu \tilde{\Lambda}(x), \quad (2.8)$$

which means that the full symmetry of this theory is actually $U(1) \times \tilde{U}(1)$, where the tilde on the second $U(1)$ indicates it is the symmetry of the dual potential \tilde{A} . It is important to note that the physical degrees of freedom remain just either F or $*F$, not both, since F and $*F$ are related by an *algebraic* equation (2.2). The dual symmetry is there all the time but just physically not so readily detected and it means that what we call ‘electric’ or ‘magnetic’ is entirely a matter of choice.

Before we go back to discuss matter carrying charges of the gauge theory, let us first distinguish between two types of charges: sources and monopoles. These are defined with respect to the gauge field, which in turn is derivable from the gauge potential.

Source charges are those charges that give rise to a nonvanishing divergence of the field. For example, the electric current j due to the presence of the electric charge e occurs on the right hand side of the first Maxwell equation, and is given in the quantum case by

$$j^\mu = e \bar{\psi} \gamma^\mu \psi. \quad (2.9)$$

In the Yang–Mills case with general nonabelian gauge group G , the first Maxwell equation is replaced by the Yang–Mills equation:

$$D_\nu F^{\mu\nu} = -j^\mu, \quad j^\mu = g \bar{\psi} \gamma^\mu \psi, \quad (2.10)$$

where we define the covariant derivative D by

$$D_\mu F^{\mu\nu} = \partial_\mu F^{\mu\nu} - ig [A_\mu, F^{\mu\nu}]. \quad (2.11)$$

Monopole charges, on the other hand, are topological obstructions specified geometrically by nontrivial G -bundles over every 2-sphere S^2 surrounding the charge². They are classified by elements of $\pi_1(G)$, the fundamental group of G , that is, classes of closed loops in the group manifold which can be continuously deformed into one another. They are typified by the (abelian) magnetic monopole as first discussed by Dirac in 1931 [13]. A nonabelian example is that of $SO(3)$, where the monopole charges are just denoted by a sign: ± 1 , with $+1$ corresponding to the vacuum and -1 to the monopole. Figure 1 illustrates this case. Moreover, we can obtain the *Dirac quantiza-*

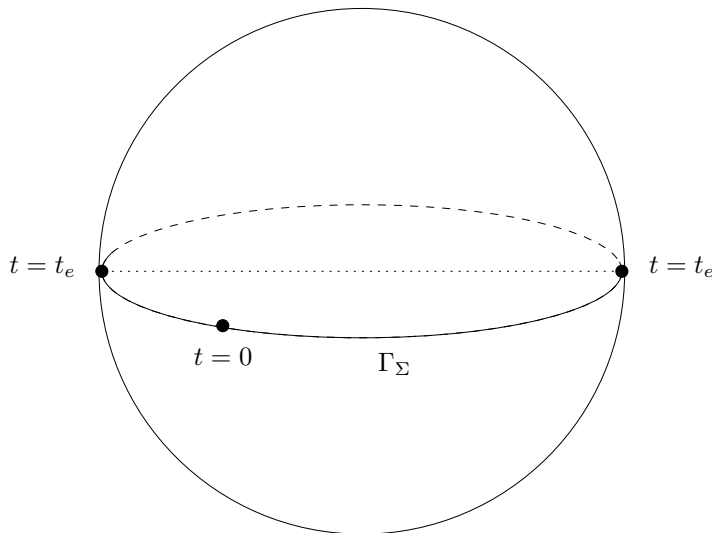


Figure 1: An $SO(3)$ monopole.

²For the nonmathematical reader, a more intuitive picture of a monopole as topological obstruction can be found in, for example, [14], section 2.1.

tion condition quite easily from the definition of the monopole, which in the abelian case is:

$$e\tilde{e} = 2\pi, \tag{2.12}$$

and in the nonabelian case is:

$$g\tilde{g} = 4\pi, \tag{2.13}$$

the difference between the two cases being only a matter of conventional normalization [14, 15].

Now in the presence of electric charges, the Maxwell equations appear usually as

$$\partial_\nu {}^*F^{\mu\nu} = 0 \tag{2.14}$$

$$\partial_\nu F^{\mu\nu} = -j^\mu. \tag{2.15}$$

The apparent asymmetry in these equations comes from the experimental fact that there is only one type of charges observed in nature which we choose to regard as a source of the field F (or, equivalently but unconventionally, as a monopole of the field *F). But as we see by dualizing equations (2.14) and (2.15), that is, by interchanging the role of electricity and magnetism in relation to F , we could equally have thought of these instead as source charges of the field *F (or, similarly to the above, as monopoles of F):

$$\partial_\nu {}^*F^{\mu\nu} = -\tilde{j}^\mu \tag{2.16}$$

$$\partial_\nu F^{\mu\nu} = 0. \tag{2.17}$$

And if both electric and magnetic charges existed in nature, then we would have the dual symmetric pair:

$$\partial_\nu {}^*F^{\mu\nu} = -\tilde{j}^\mu \tag{2.18}$$

$$\partial_\nu F^{\mu\nu} = -j^\mu. \tag{2.19}$$

The duality in the presence of matter goes in fact much deeper, as can be seen if we use the Wu–Yang criterion [16, 17] to derive the Maxwell equations³. Consider first pure electromagnetism. The free Maxwell action is:

$$\mathcal{A}_F^0 = -\frac{1}{4} \int F_{\mu\nu} F^{\mu\nu}. \tag{2.20}$$

³What we present here is not the textbook derivation of Maxwell’s equations from an action, but we consider this method to be much more intrinsic and geometric.

The true variables of the (quantum) theory are the A_μ , so in (2.20) we should put in a constraint to say that $F_{\mu\nu}$ is the curl of A_μ (2.5). This can be viewed as a topological constraint, because it is precisely equivalent to (2.3). Using the method of Lagrange multipliers, we form the constrained action

$$\mathcal{A} = \mathcal{A}_F^0 + \int \lambda_\mu (\partial_\nu {}^*F^{\mu\nu}), \quad (2.21)$$

which we can now vary with respect to $F_{\mu\nu}$, obtaining

$$F^{\mu\nu} = 2 \epsilon^{\mu\nu\rho\sigma} \partial_\rho \lambda_\sigma \quad (2.22)$$

which implies (2.4). Moreover, the Lagrange multiplier λ is exactly the dual potential \tilde{A} . The derivation is entirely dual symmetric, since we can equally well use (2.4) as constraint for the action \mathcal{A}_F^0 , now considered as a functional of ${}^*F^{\mu\nu}$:

$$\mathcal{A}_F^0 = \frac{1}{4} \int {}^*F_{\mu\nu} {}^*F^{\mu\nu}, \quad (2.23)$$

and obtain (2.3) as the equation of motion.

This method applies to the interaction of charges and fields as well. In this case we start with the free field plus free particle action:

$$\mathcal{A}^0 = \mathcal{A}_F^0 + \int \bar{\psi} (i\partial_\mu \gamma^\mu - m) \psi, \quad (2.24)$$

where we assume the free particle m to satisfy the Dirac equation. To fix ideas, let us regard this particle carrying an electric charge e as a monopole of the potential \tilde{A}_μ . Then the constraint we put in is (2.15):

$$\mathcal{A}' = \mathcal{A}^0 + \int \tilde{\lambda}_\mu (\partial_\nu F^{\mu\nu} + j^\mu). \quad (2.25)$$

Varying with respect to *F gives us (2.14), and varying with respect to $\bar{\psi}$ gives

$$(i\partial_\mu \gamma^\mu - m) \psi = -e A_\mu \gamma^\mu \psi. \quad (2.26)$$

So the complete set of equations for a Dirac particle carrying an electric charge e in an electromagnetic field is (2.14), (2.15) and (2.26). The duals of these equations will describe the dynamics of a Dirac magnetic monopole in an electromagnetic field.

We see from this that the Wu–Yang criterion actually gives us an intuitively clear picture of interactions. The assertion that there is a monopole

at a certain spacetime point x means that the gauge field on a 2-sphere surrounding x has to have a certain topological configuration (e.g. giving a nontrivial bundle of a particular class), and if the monopole moves to another point, then the gauge field will have to rearrange itself so as to maintain the same topological configuration around the new point. There is thus naturally a coupling between the gauge field and the position of the monopole, or in physical language a topologically induced interaction between the field and the charge [16]. Furthermore, this treatment of interaction between field and matter is entirely dual symmetric.

The next natural step is to generalize this duality to the nonabelian Yang–Mills case. Although there is no difficulty in defining $*F^{\mu\nu}$, which is again given by (2.2), we immediately come to difficulties in the relation between field and potential:

$$F_{\mu\nu}(x) = \partial_\nu A_\mu(x) - \partial_\mu A_\nu(x) + ig [A_\mu(x), A_\nu(x)]. \quad (2.27)$$

First of all, despite appearances the Yang–Mills equation (in the free field case)

$$D_\nu F^{\mu\nu} = 0 \quad (2.28)$$

and the Bianchi identity

$$D_\nu *F^{\mu\nu} = 0 \quad (2.29)$$

are not dual-symmetric, because the correct dual of the Yang–Mills equation ought to be

$$\tilde{D}_\nu *F^{\mu\nu} = 0, \quad (2.30)$$

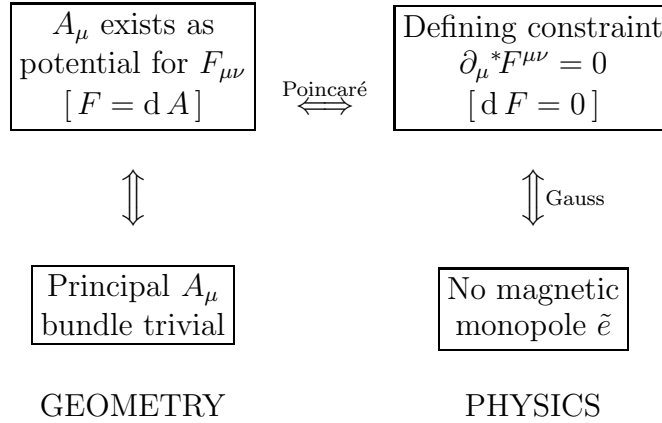
where \tilde{D}_ν is the covariant derivative corresponding not to A_ν but to a dual potential. Secondly, the Yang–Mills equation, unlike its abelian counterpart (2.4), says nothing about whether the 2-form $*F$ is closed or not. Nor is the relation (2.27) about exactness at all. In other words, the Yang–Mills equation does not guarantee the existence of a dual potential, in contrast to the Maxwell case. In fact, Gu and Yang [18] have constructed a counterexample. Because the true variables of a gauge theory are the potentials and not the fields, this means that Yang–Mills theory is *not symmetric* under the Hodge star operation (2.2) which in the abelian case gives us the duality transform.

Nevertheless, electric–magnetic duality is a very useful physical concept. So one may wish to seek a more general duality transform ($\tilde{\quad}$) satisfying the following properties:

1. $(\tilde{\quad})^{\sim\sim} = \pm(\quad)$,

2. electric field $F_{\mu\nu} \xleftrightarrow{\sim} \text{magnetic field } \tilde{F}_{\mu\nu}$,
3. both A_μ and \tilde{A}_μ exist as potentials (away from charges),
4. magnetic charges are monopoles of A_μ , and electric charges are monopoles of \tilde{A}_μ ,
5. \sim reduces to $*$ in the abelian case.

One way to do so is to study the Wu–Yang criterion more closely. This reveals the concept of charges as topological constraints to be crucial even in the pure field case, as can be seen in the diagram below:



The point to stress is that, in the above abelian case, the condition for the absence of a topological charge (a monopole) exactly removes the redundancy of the variables $F_{\mu\nu}$, and hence recovers the potential A_μ .

Now the nonabelian monopole charge was defined topologically as an element of $\pi_1(G)$, and this definition also holds in the abelian case of $U(1)$, with $\pi_1(U(1)) = \mathbb{Z}$. So the first task is to write down a condition for the absence of a nonabelian monopole.

Consider the gauge invariant Dirac phase factor (or holonomy) $\Phi(C)$ of a loop C , which can be written symbolically as a path-ordered exponential:

$$\Phi[\xi] = P_s \exp ig \int_0^{2\pi} ds A_\mu(\xi(s)) \dot{\xi}^\mu(s), \quad (2.31)$$

where we parametrize the loop C :

$$C : \quad \{\xi^\mu(s) : s = 0 \rightarrow 2\pi, \xi(0) = \xi(2\pi) = \xi_0\}, \quad (2.32)$$

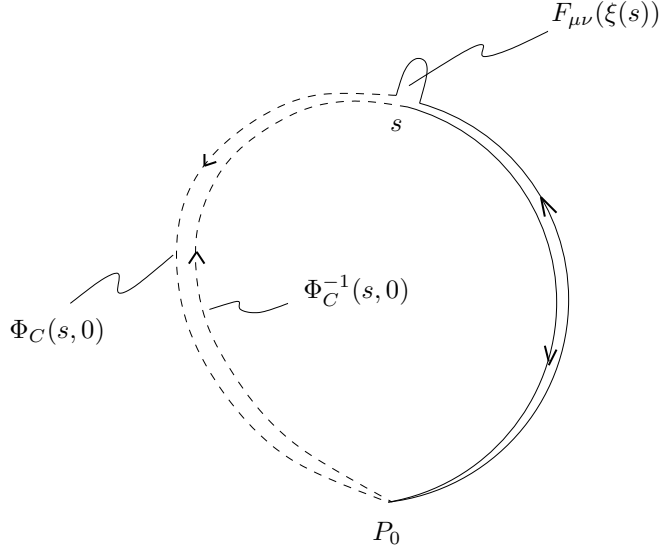


Figure 2: Illustration for ‘loop connection’.

and a dot denotes differentiation with respect to the parameter s . We thus regard loop variables in general as functionals of continuous piecewise smooth functions ξ of s . In this way, loop derivatives and loop integrals are just functional derivatives and functional integrals. This means that loop derivatives $\delta_\mu(s)$ are defined by a regularization procedure approximating delta functions with finite bump functions and then taking limits in a definite order.

Following Polyakov [19] we introduce the logarithmic loop derivative of $\Phi[\xi]$:

$$F_\mu[\xi|s] = \frac{i}{g} \Phi^{-1}[\xi] \delta_\mu(s) \Phi[\xi], \quad (2.33)$$

which acts as a kind of ‘connection’ in loop space since it tells us how the phase of $\Phi[\xi]$ changes from one loop to a neighbouring loop, as illustrated in Figure 2. One can go a step further and define its ‘curvature’ in direct analogy with $F_{\mu\nu}(x)$:

$$G_{\mu\nu}[\xi|s] = \delta_\nu(s) F_\mu[\xi|s] - \delta_\mu(s) F_\nu[\xi|s] + ig [F_\mu[\xi|s], F_\nu[\xi|s]]. \quad (2.34)$$

It can be shown that using the $F_\mu[\xi|s]$ we can rewrite the Yang–Mills action as

$$\mathcal{A}_F^0 = -\frac{1}{4\pi N} \int \delta\xi \int_0^{2\pi} ds \text{Tr}\{F_\mu[\xi|s] F^\mu[\xi|s]\} |\dot{\xi}(s)|^{-2}, \quad (2.35)$$

where the normalization factor \bar{N} is an infinite constant. However, the true variables of the theory are still the A_μ . They represent 4 functions of a real variable, whereas the loop connections represent 4 functionals of the real function $\xi(s)$. Just as in the case of the $F_{\mu\nu}$, these $F_\mu[\xi|s]$ have to be constrained so as to recover A_μ , but this time much more severely.

It turns out that in pure Yang–Mills theory, the constraint that says there are no monopoles:

$$G_{\mu\nu}[\xi|s] = 0 \tag{2.36}$$

removes also the redundancy of the loop variables, exactly as in the abelian case. That this condition is necessary is easy to see, by simple algebra. The proof of the converse of this “extended Poincaré lemma” [20, 14] is fairly lengthy and will not be presented. Granted this, we can now apply the Wu–Yang criterion to the action (2.35) and derive the Polyakov equation:

$$\delta_\mu(s)F^\mu[\xi|s] = 0, \tag{2.37}$$

which is the loop version of the Yang–Mills equation.

In the presence of a monopole charge $-$, if we use the $SO(3)$ example as an illustration, the constraint (2.36) will have a nonzero right hand side:

$$G_{\mu\nu}[\xi|s] = -J_{\mu\nu}[\xi|s]. \tag{2.38}$$

The loop current $J_{\mu\nu}[\xi|s]$ can be written down explicitly. However, its global form is much easier to understand. Recall that $F^\mu[\xi|s]$ can be thought of as a loop connection, for which we can form *its* ‘holonomy’. This is defined for a closed (spatial) surface Σ (enclosing the monopole), parametrized by a family of closed curves $\xi_t(s)$, $t = 0 \rightarrow 2\pi$. The ‘holonomy’ Θ_Σ is then the total change in phase of $\Phi[\xi_t]$ as $t \rightarrow 2\pi$, and thus equals the charge $-$.

To formulate an electric–magnetic duality which is applicable to non-abelian theory one defines yet another set of loop variables. Instead of the Dirac phase factor $\Phi[\xi]$ for a complete curve (2.31) we consider the parallel phase transport for part of a curve from s_1 to s_2 :

$$\Phi_\xi(s_2, s_1) = P_s \exp ig \int_{s_1}^{s_2} ds A_\mu(\xi(s)) \dot{\xi}^\mu(s). \tag{2.39}$$

Then the new variables are defined as:

$$E_\mu[\xi|s] = \Phi_\xi(s, 0) F_\mu[\xi|s] \Phi_\xi^{-1}(s, 0). \tag{2.40}$$

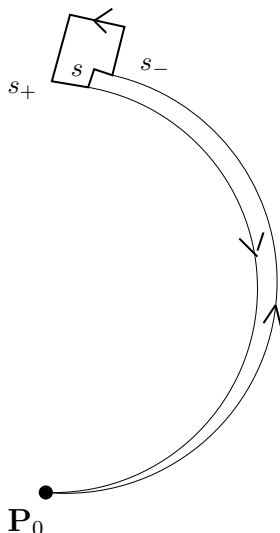


Figure 3: Illustration of the segmental variable E_μ .

These are not gauge invariant like $F_\mu[\xi|s]$ and may not be as useful in general but seem more convenient for dealing with duality. A schematic representation is given in Figure 3.

Using these variables, we now define [21] their *dual* $\tilde{E}_\mu[\eta|t]$ as:

$$\begin{aligned} & \omega^{-1}(\eta(t)) \tilde{E}_\mu[\eta|t] \omega(\eta(t)) \\ = & -\frac{2}{N} \epsilon_{\mu\nu\rho\sigma} \dot{\eta}^\nu(t) \int \delta\xi ds E^\rho[\xi|s] \dot{\xi}^\sigma(s) \xi^{-2}(s) \delta(\xi(s) - \eta(t)), \end{aligned} \quad (2.41)$$

where $\omega(x)$ is a (local) rotation matrix transforming from the frame in which the orientation in internal symmetry space of the fields $E_\mu[\xi|s]$ are measured to the frame in which the dual fields $\tilde{E}_\nu[\eta|t]$ are measured. It can be shown that this dual transform satisfies all the 5 required conditions we listed before.

Electric–magnetic duality in Yang–Mills theory is now fully re-established using this generalized duality. We have the following dual pairs of equations:

$$\delta_\nu E_\mu - \delta_\mu E_\nu = 0, \quad (2.42)$$

$$\delta^\mu E_\mu = 0; \quad (2.43)$$

and dually

$$\delta^\mu \tilde{E}_\mu = 0, \quad (2.44)$$

$$\delta_\nu \tilde{E}_\mu - \delta_\mu \tilde{E}_\nu = 0. \quad (2.45)$$

Equation (2.42) guarantees that the potential A exists, and so is equivalent to (2.36), and hence is the nonabelian analogue of (2.3); while equation (2.43) is equivalent to the Polyakov version of Yang–Mills equation (2.37), and hence is the nonabelian analogue of (2.4). Equation (2.44) is equivalent by duality to (2.42) and is the dual Yang–Mills equation. Similarly equation (2.45) is equivalent to (2.43), and guarantees the existence of the dual potential \tilde{A} .

The treatment of charges using the Wu–Yang criterion also follows the abelian case, and will not be further elaborated here. For this and further details the reader is referred to the original papers [21].

Also just as in the abelian case, the gauge symmetry is doubled: from the group G we deduce that the full gauge symmetry is in fact $G \times \tilde{G}$, but that the physical degrees of freedom remain the same.

3 The Dualized Standard Model

That duality exists also for nonabelian Yang–Mills theory, as outlined in the last section, is of basic theoretical interest, and is likely to have repercussions in many areas of physics. So far, however, the applications we have made are concentrated in the problem of fermion generations where, as we shall see, the consequences are both concrete and immediate. The reason is as follows.

We recall that according to present experiment, fermions occur in 3 and apparently only 3 generations, which suggests a hidden 3-fold symmetry, known in the literature for historical reasons as “horizontal symmetry” [22]. This symmetry must be broken, and in a rather unusual manner, given the peculiar hierarchical fermion mass spectrum quoted above (1.1). In most previous studies, the existence as well as the breaking of this horizontal symmetry have to be taken as inputs thus reducing the overall predictive power. But with the nonabelian duality derived above, the idea takes on a more concrete shape. First, dual to colour $SU(3)$, one knows that there is automatically another, dual colour symmetry $\widetilde{SU}(3)$ bearing a similar relationship to colour as magnetism bears to electricity. Secondly, one knows that this dual colour symmetry is broken. This follows from a result of ’t Hooft [23] which says that if colour $SU(3)$ is confined, as it is, then its dual is necessarily broken. Indeed, using the machinery developed in Section 2, it can be shown [15] that the Wilson operators:

$$A(C) = \text{Tr} \left[P \exp ig \oint_C A_i(x) dx^i \right], \quad (3.1)$$

and:

$$B(C) = \text{Tr} \left[P \exp i\tilde{g} \oint_C \tilde{A}_i(x) dx^i \right], \quad (3.2)$$

constructed from respectively the colour potential $A_i(x)$ and the dual colour potential $\tilde{A}_i(x)$, satisfy the commutation relation used by 't Hooft to derive his result, namely:

$$A(C)B(C') = B(C')A(C) \exp(2\pi il/N) \quad (3.3)$$

for $SU(N)$ gauge group and for any 2 spatial loops C and C' with linking number l .

In other words, this means that, by virtue of nonabelian duality, there is within the Standard Model framework already hidden a broken 3-fold symmetry corresponding to dual colour which can play the role of the horizontal symmetry for generations. That being the case, it seems natural to identify dual colour $\widetilde{SU}(3)$ as such. Indeed, if one does not do so, one may be at a loss as to what physical significance to assign to this symmetry which, according to nonabelian duality, will be there in any case. But with this identification, one may claim that nonabelian duality predicts the existence of 3 and only 3 generations as experimentally observed.

The cited result of 't Hooft shows that the $\widetilde{SU}(3)$ dual colour symmetry is broken, but offers no hint as to the Higgs mechanism for breaking it. Interestingly, however, the framework developed above for nonabelian duality itself suggests natural candidates for the Higgs fields. It was noted before [24] that the transformation matrix $\omega(x)$ relating the colour to dual colour frame which appears in the dual transform (2.41) has to be patched (or alternatively to carry a Dirac string) in the presence of charges, and in monopole theory, according to Wu and Yang [16], it is the patching in gauge fields in the presence of charges which gives rise to interactions between them. Hence, the observation that $\omega(x)$ be patched suggests that its elements, or else the colour and dual colour frame vectors from which it is constructed, can play a dynamical role and be considered for promotion to physical fields. The idea of promoting frame vectors to be physical fields is of course not new, a well-known previous example being the “vierbeins” in the Einstein-Cartan-Kibble-Sciama formulation of relativity [25]. If one were to promote the dual colour frame vectors to fields, then they would have the appropriate properties of the Higgs fields necessary for breaking the dual colour symmetry, being triplets of dual colour, space-time scalars and having finite “classical” lengths.

The starting assumption of our Dualized Standard Model scheme is then to make the identifications of dual colour to generations and of frame vectors to Higgs fields for breaking the dual colour symmetry. Apart from the practical advantages to be detailed below, this has, to us, the aesthetic appeal of assigning to both generations and Higgs fields a geometric significance which they so sadly lack in our conventional formulation of the Standard Model.

To proceed further, one needs an action, in particular the couplings of the Higgs fields, i.e. the dual colour frame vectors, first to themselves and second to the fermions. The dual colour frame vectors represent 3 complex triplet scalar fields $\phi_a^{(a)}$, $(a) = 1, 2, 3$, where $a = 1, 2, 3$ are dual colour or generation indices. Being frame vectors, and therefore having equal status, they ought, we argued [26], to appear in the action symmetrically. We sought thus to construct with these a Higgs potential which is renormalizable, $\widetilde{SU}(3)$ invariant, and symmetric under permutations of the 3 triplets but having a degenerate vacuum which breaks both the dual colour $\widetilde{SU}(3)$ symmetry and the permutation symmetry spontaneously. We proposed in [26] the following:

$$V[\phi] = -\mu \sum_{(a)} |\phi^{(a)}|^2 + \lambda \left\{ \sum_{(a)} |\phi^{(a)}|^2 \right\}^2 + \kappa \sum_{(a) \neq (b)} |\bar{\phi}^{(a)} \cdot \phi^{(b)}|. \quad (3.4)$$

It has degenerate vacua of the form:

$$\phi^{(1)} = \zeta \begin{pmatrix} x \\ 0 \\ 0 \end{pmatrix}, \quad \phi^{(2)} = \zeta \begin{pmatrix} 0 \\ y \\ 0 \end{pmatrix}, \quad \phi^{(3)} = \zeta \begin{pmatrix} 0 \\ 0 \\ z \end{pmatrix}, \quad (3.5)$$

with

$$\zeta = \sqrt{\mu/2\lambda}, \quad (3.6)$$

and x, y, z all real and positive, satisfying:

$$x^2 + y^2 + z^2 = 1, \quad (3.7)$$

which breaks the permutation symmetry between the ϕ 's, and also the $\widetilde{SU}(3)$ gauge symmetry completely. In fact, all 9 (dual) gauge bosons in the theory acquire a mass, eating up all but 9 of the original 18 real Higgs modes.

Further, by analogy to the electroweak theory we proposed [26] the following Yukawa coupling to the fermions fields, again symmetric under permutations of the 3 Higgs triplets:

$$\sum_{(a)[b]} Y_{[b]} \bar{\psi}_L^a \phi_a^{(a)} \psi_R^{[b]} + \text{h.c.}, \quad (3.8)$$

where ψ_L^a , $a = 1, 2, 3$ is the left-handed fermion field appearing as a dual colour triplet, and $\psi_R^{[b]}$, $[b] = 1, 2, 3$, are 3 right-handed fermion fields, each appearing as a dual colour singlet⁴.

Neither the Higgs potential (3.4) above nor the Yukawa coupling (3.8) can claim to be unique as implementations of the duality ideas introduced before, and have thus to be regarded at present as phenomenological constructs pending justification on a more theoretical basis, which we have some hope of supplying in future but have not yet succeeded in doing so. They may thus possibly be subject to modifications. However, although the successes we shall show later in reproducing the fermion mass and mixing patterns have been obtained with these explicit constructs, we shall see indications that the most salient features could probably be retained under more general conditions.

For the moment, however, let us continue with the explicit constructs (3.4) and (3.8) and explore the consequences. First, by inserting the vacuum expectation values (3.5) of the Higgs fields $\phi_a^{(a)}$ into the Yukawa coupling (3.8), one obtains the fermion mass matrix at tree level:

$$\tilde{m} \frac{1}{2}(1 + \gamma_5) + \tilde{m}^\dagger \frac{1}{2}(1 - \gamma_5), \quad (3.9)$$

where \tilde{m} is a factorized matrix:

$$\tilde{m} = \zeta \begin{pmatrix} x \\ y \\ z \end{pmatrix} (a, b, c), \quad (3.10)$$

with a, b, c being the Yukawa couplings $Y_{[b]}$. For future discussion it is convenient, following Weinberg [27], to rewrite the mass matrix \tilde{m} in a hermitian form, basically replacing \tilde{m} by $\sqrt{\tilde{m}\tilde{m}^\dagger}$. This can always be done by a re-belling of the right-handed singlet fields $\psi_R^{[b]}$ without in any way affecting the physics, as will be explicitly demonstrated for a general mass matrix in the next section. Applied to \tilde{m} above, one obtains:

$$m = m_T \begin{pmatrix} x \\ y \\ z \end{pmatrix} (x, y, z), \quad (3.11)$$

⁴We note that in order to have dual colour triplets occurring as monopoles of colour as we do here, the colour $SU(3)$ group has to be imbedded in a larger theory as indeed it is in the Standard Model. This also makes it possible to have 9 gauge bosons acquiring mass, as stated above. For a detailed explanation of this point, see e.g. [26].

which gives the physical states directly as the mass eigenstates.

We note first that apart from the proportionality factor m_T for $T = U, D, L, N$, this tree-level mass matrix is the same for all the 4 fermion species, which means in particular that at tree-level the up and down mass matrices are aligned, hence giving no mixing at zeroth order, which is no bad approximation at least for quarks. Secondly, we note that this matrix is of rank 1, having thus only one nonzero eigenvalue, which we may interpret as an embryonic version of fermion mass hierarchy and is a consequence of the stipulated condition that our action be invariant under permutations of the three Higgs fields. In other words, one begins to see already the empirical fermion mass and mixing patterns taking shape.

One can do better, however. Given the Higgs potential (3.4) and the Yukawa coupling (3.8), it is only a matter of working through some algebra [28] to arrive at the following mass spectrum for the remaining 9 Higgs bosons:

$$\begin{aligned}
K = 1 : & \quad 8\lambda\zeta^2(x^2 + y^2 + z^2), \\
K = 2 : & \quad 4\kappa\zeta^2(y^2 + z^2), \\
K = 3 : & \quad 4\kappa\zeta^2(y^2 + z^2), \\
K = 4 : & \quad 4\kappa\zeta^2(z^2 + x^2), \\
K = 5 : & \quad 4\kappa\zeta^2(z^2 + x^2), \\
K = 6 : & \quad 4\kappa\zeta^2(x^2 + y^2), \\
K = 7 : & \quad 4\kappa\zeta^2(x^2 + y^2), \\
K = 8 : & \quad 0, \\
K = 9 : & \quad 0,
\end{aligned} \tag{3.12}$$

and the following for their couplings to fermions:

$$\bar{\Gamma}_K = \bar{\gamma}_K \frac{1}{2}(1 + \gamma_5) + \bar{\gamma}_K^\dagger \frac{1}{2}(1 - \gamma_5), \tag{3.13}$$

where:

$$\bar{\gamma}_K = \rho |v_K\rangle \langle v_1|, \tag{3.14}$$

and:

$$|v_1\rangle = \begin{pmatrix} x \\ y \\ z \end{pmatrix},$$

$$\begin{aligned}
|v_2\rangle &= \frac{1}{\sqrt{y^2 + z^2}} \begin{pmatrix} 0 \\ y \\ z \end{pmatrix}, \\
|v_3\rangle &= \frac{i}{\sqrt{y^2 + z^2}} \begin{pmatrix} 0 \\ y \\ -z \end{pmatrix}, \\
|v_4\rangle &= \frac{1}{\sqrt{z^2 + x^2}} \begin{pmatrix} x \\ 0 \\ z \end{pmatrix}, \\
|v_5\rangle &= \frac{i}{\sqrt{z^2 + x^2}} \begin{pmatrix} -x \\ 0 \\ z \end{pmatrix}, \\
|v_6\rangle &= \frac{1}{\sqrt{x^2 + y^2}} \begin{pmatrix} x \\ y \\ 0 \end{pmatrix}, \\
|v_7\rangle &= \frac{i}{\sqrt{x^2 + y^2}} \begin{pmatrix} x \\ -y \\ 0 \end{pmatrix}, \\
|v_8\rangle &= -\beta \begin{pmatrix} y - z \\ z - x \\ x - y \end{pmatrix}, \\
|v_9\rangle &= \beta \begin{pmatrix} 1 - x(x + y + z) \\ 1 - y(x + y + z) \\ 1 - z(x + y + z) \end{pmatrix}, \tag{3.15}
\end{aligned}$$

with

$$\beta^{-2} = 3 - (x + y + z)^2. \tag{3.16}$$

Given the above information, it is then possible to calculate the loop corrections with these dual colour Higgs bosons exchanged, in particular the 1-loop insertion of Figure 4 to the fermion propagator where the dashed line represents one of the Higgs boson states listed in (3.12). Even at the 1-loop level, of course, there will be many more diagrams giving insertions to the fermion propagator but these will all be seen to yield but negligible contributions to calculating the fermion mass and mixing patterns which is our main concern here and can thus for the present be ignored. For Figure

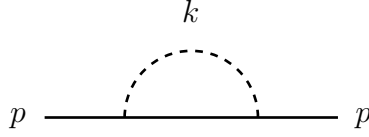


Figure 4: 1-loop insertion to the fermion propagator.

4 then, one has explicitly:

$$\Sigma(p) = \frac{i}{(4\pi)^4} \sum_K \int d^4k \frac{1}{k^2 - M_K^2} \bar{\Gamma}_K \frac{(\not{p} - \not{k}) + m}{(p - k)^2 - m^2} \bar{\Gamma}_K, \quad (3.17)$$

with m and $\bar{\Gamma}_K$ given in (3.11) and (3.13). Combining denominators by the standard Feynman parametrization and shifting the origin of the k -integration as usual, one obtains:

$$\Sigma(p) = \frac{i}{(4\pi)^4} \sum_K \int_0^1 dx \bar{\Gamma}_K \left\{ \int d^4k \frac{\not{p}(1-x) + m}{[k^2 - Q^2]^2} \right\} \bar{\Gamma}_K, \quad (3.18)$$

with

$$Q^2 = m^2x + M_K^2(1-x) - p^2x(1-x), \quad (3.19)$$

where we note that m , being a matrix in generation space, cannot be commuted through the couplings $\bar{\Gamma}_K$. The integration over k in (3.18) is divergent and has to be regularized. Following the standard dimensional regularization procedure, one obtains:

$$\Sigma(p) = -\frac{1}{16\pi^2} \sum_K \int_0^1 dx \bar{\Gamma}_K \{ \bar{C} - \ln(Q^2/\mu^2) \} \{ \not{p}(1-x) + m \} \bar{\Gamma}_K, \quad (3.20)$$

with \bar{C} being the divergent constant:

$$\bar{C} = \lim_{d \rightarrow 4} \left[\frac{1}{2 - d/2} - \gamma \right], \quad (3.21)$$

to be subtracted in the standard $\overline{\text{MS}}$ scheme.

To extract the renormalized mass matrix:

$$m' = m + \delta m \tag{3.22}$$

from $\Sigma(p)$, one normally puts in the denominator $p^2 = m^2$ and commutes \not{p} in the numerator to the left or right and replace by m [27]. However, m being now a matrix, this operation is a little more delicate. In order to maintain the “hermitian”, left–right symmetric form (3.11) for the renormalized mass matrix m' , we split the \not{p} term into two halves, commuting half to the left and half to the right before replacing by m , and hence obtain for δm the following:

$$\begin{aligned} \delta m = & \frac{\rho^2}{16\pi^2} \sum_K \int_0^1 dx \{ \bar{\gamma}_K m [\bar{C} - \ln(Q_0^2/\mu^2)] \bar{\gamma}_K \frac{1}{2}(1 + \gamma_5) \\ & + \bar{\gamma}_K^\dagger m [\bar{C} - \ln(Q_0^2/\mu^2)] \bar{\gamma}_K^\dagger \frac{1}{2}(1 - \gamma_5) \} \\ & + \frac{\rho^2}{32\pi^2} \sum_K \int_0^1 dx (1 - x) m \{ \bar{\gamma}_K^\dagger [\bar{C} - \ln(Q_0^2/\mu^2)] \bar{\gamma}_K \frac{1}{2}(1 + \gamma_5) \\ & + \bar{\gamma}_K [\bar{C} - \ln(Q_0^2/\mu^2)] \bar{\gamma}_K^\dagger \frac{1}{2}(1 - \gamma_5) \} \\ & + \frac{\rho^2}{32\pi^2} \sum_K \int_0^1 dx (1 - x) \{ \bar{\gamma}_K [\bar{C} - \ln(Q_0^2/\mu^2)] \bar{\gamma}_K^\dagger \frac{1}{2}(1 + \gamma_5) \\ & + \bar{\gamma}_K^\dagger [\bar{C} - \ln(Q_0^2/\mu^2)] \bar{\gamma}_K \frac{1}{2}(1 - \gamma_5) \} m, \end{aligned} \tag{3.23}$$

with

$$Q_0^2 = Q^2|_{p^2=m^2} = m^2 x^2 + M_K^2(1 - x). \tag{3.24}$$

Again a relabelling of the right-handed fermion fields is required to bring the renormalized mass matrix back to the hermitian form (3.11) of Weinberg adopted here.

The expression (3.23) for the 1-loop correction to the mass matrix is a little complicated, but for the consideration of the fermion mass and mixing patterns of main concern in this paper, the only relevant terms in (3.23) are those proportional to $\ln \mu^2$, with μ being the renormalization scale. The reason is that the remainder can readily be shown [28, 29] to be of order m^2/M^2 , where M is a mass scale bounded by present experimental limits on flavour-violation to be of order 100 TeV [28, 30], to which questions we shall

return at the end of these lectures in section 7. Keeping then only these $\ln \mu^2$ terms and summing over all the Higgs bosons labelled by K , one obtains [28]:

$$m' = m'_T \begin{pmatrix} x' \\ y' \\ z' \end{pmatrix} (x', y', z'), \quad (3.25)$$

where the vector (x', y', z') satisfies an RG-type equation of the following form:

$$\frac{d}{d(\ln \mu^2)} \begin{pmatrix} x' \\ y' \\ z' \end{pmatrix} = \frac{3}{64\pi^2} \rho^2 \begin{pmatrix} x'_1 \\ y'_1 \\ z'_1 \end{pmatrix}, \quad (3.26)$$

with

$$x'_1 = \frac{x'(x'^2 - y'^2)}{x'^2 + y'^2} + \frac{x'(x'^2 - z'^2)}{x'^2 + z'^2}, \quad \text{cyclic}, \quad (3.27)$$

and ρ being the Yukawa coupling strength⁵.

We notice first that the renormalized mass matrix (3.25) remains of the factorized form. This result is independent of whether terms of order m^2/M^2 are included or not and will hold even with the inclusion of diagrams other than the calculated Higgs loop of Figure 4. It holds simply by virtue of the also factorized form of the Higgs coupling as deduced from (3.8), and of the fact that the dual colour gauge bosons couple only to left-handed fermions which are dual colour triplets but not to right-handed fermions which are dual colour singlets [28]. Secondly, we note that to the very good approximation of neglecting quantities of order m^2/M^2 , the vectors (x', y', z') are identical for all 4 fermion species U, D, L, N , so that the mass matrices are still the same apart from the normalisation m'_T . (In principle, the Yukawa coupling strength ρ appearing in equation (3.26) can also depend on the fermion species, but for reasons of consistency [28, 32] to be reviewed later, they have to be equal in the DSM scheme.) The resulting picture is thus extremely simple, and formally similar to that at tree level. There is, however, a very important difference, namely that, in contrast to the tree-level mass matrix (3.11), the vector (x', y', z') factored from the renormalized mass

⁵There was an error in [28] which gave the coefficient on the right of eq. (3.26) as $5/(64\pi^2)$ instead of $3/(64\pi^2)$ as in here. This was due to a sign error in the first term on the right of eq. (4.14) of [28] arising from a misprint in the formula for $\Sigma^{(\phi^1)}$ in eq. (3.2) of [27] quoted there. However, apart from the fact that the numerical values given for the parameter ρ in eq. (6.8) in [28] should be increased by a factor $\sqrt{5/3}$, no other results given in that paper or in its sequels such as [31] are affected by this error.

matrix is no longer constant but depends on scale via the equations (3.26) and (3.27). It changes not only in length but also in direction, which means that the mass matrix, apart from running in normalization, also changes in orientation, that is, rotates, with changing scale. And this difference, as we shall see in the next section, is enough not only to give nontrivial mixing and nonzero masses to the lower generations, both of which were missing in the tree approximation, but also to offer an immediate explanation for almost all the salient features of the experimentally observed fermion mass and mixing patterns quoted in section 1, which had seemed so mysterious before.

4 The Rotating Mass Matrix and its Implications

That the renormalized mass matrix should change with scale, like the coupling constant and other field quantities, is of course no surprise, and that it should rotate also is not peculiar just to the DSM scheme but happens already in the Standard Model as conventionally formulated [33, 26], although the rotation there is very weak and its effects are thus for most applications negligible. What is perhaps not widely recognized, however, is that when the mass matrix does rotate, then some of our usual kinematical concepts such as particle masses, state vectors and mixing parameters will have to be refined. This is a matter of principle which will have to be faced in whatever situation where the mass matrix rotates, however weakly, not just in the DSM scheme being considered.

The situation being unfamiliar, it would be worthwhile to examine it afresh starting from basics and in terms of a general rotating mass matrix before specializing later to the DSM case. Let us start then with a fermion mass matrix traditionally defined by a term in the action of the form:

$$\bar{\psi}_L^0 \tilde{m} \psi_R^0 + \text{h.c.}, \quad (4.1)$$

where ψ_L^0 and ψ_R^0 represent respectively the left- and right-handed fermion field, each being a vector in 3-dimensional flavour space, here given in the weak gauge basis, and \tilde{m} is a 3×3 (complex) matrix. The matrix \tilde{m} can always be diagonalized as follows:

$$U_L^\dagger \tilde{m} U_R = \text{diag} \{m_1, m_2, m_3\} \quad (4.2)$$

with U_L, U_R unitary and m_i taken real. Thus in terms of the fields:

$$\psi_L = U_L^\dagger \psi_L^0; \quad \psi_R = U_R^\dagger \psi_R^0, \quad (4.3)$$

the term (4.1) in the action takes on the diagonal form:

$$\bar{\psi}_L \text{diag} \{m_1, m_2, m_3\} \psi_R. \quad (4.4)$$

When the mass matrix \tilde{m} is constant in orientation with respect to scale change, i.e. in our language here, when the mass matrix does not rotate, which is the simple case usually considered, then the particle masses of the 3 flavour states are just given by the diagonal values m_i . The above apply to both up and down quarks in the case of quarks, and to both charged leptons and neutrinos in the case of leptons. Hence, from the mass matrix, one obtains for the up and down states each a diagonalizing matrix U_L which we can denote respectively as U_L and U'_L . Again, in the simple case when the mass matrices do not rotate, then the mixing matrix between up and down states (i.e. CKM [3] for quarks and MNS [4] for leptons) is just given by [34]:

$$V = U_L U'^{\dagger}_L. \quad (4.5)$$

For our discussion here, as mentioned already in (3.11), it is more convenient to work with an equivalent form of the mass matrix adopted by Weinberg in [27]. Since the right-handed fermion fields are flavour singlets, they can be arbitrarily relabelled without changing any of the physics. This is clear from the fact that the mixing matrices between up and down states depend only on U_L and not on U_R . Hence, by an appropriate relabelling of right-handed fields, explicitly by defining new right-handed fields:

$$\psi'^0_R = U_L U'^{\dagger}_R \psi^0_R, \quad (4.6)$$

one obtains (4.1) in a form in which the mass matrix becomes hermitian:

$$\bar{\psi} m \frac{1}{2} (1 + \gamma_5) \psi + \bar{\psi} m \frac{1}{2} (1 - \gamma_5) \psi = \bar{\psi} m \psi, \quad (4.7)$$

with

$$m = \tilde{m} U_R U'^{\dagger}_L. \quad (4.8)$$

This is convenient because in the simple case when the mass matrix does not rotate, the particle masses are now just the real eigenvalues of the hermitian matrix m and the state vectors of flavour states just the corresponding eigenvectors, as can readily be checked with (4.2). Furthermore, the mixing matrix between up and down states becomes just

$$V_{ij} = \langle \mathbf{v}_i | \mathbf{v}'_j \rangle, \quad (4.9)$$

with $|\mathbf{v}_i\rangle$ being the eigenvector of m for the eigenvalue m_i of the up state, and a prime denoting the corresponding quantities of the down state. In (4.9), the scalar product $\langle \mathbf{v}_i | \mathbf{v}'_j \rangle$ is of course an invariant independent of the frame in which these vectors $|\mathbf{v}_i\rangle$ are expressed.

Consider now what happens in the case when the mass matrix does rotate with changing scale as is of interest to us here. Both its eigenvalues and their corresponding eigenvectors now change with the scale so that the previous definition of these as respectively the masses and state vectors of flavour states is no longer sufficiently precise, for it will have to be specified at which scale(s) the eigenvalues and eigenvectors are to be evaluated.

In the simple case of a single generation, i.e. when the mass matrix is just a number, one is used to defining the particle mass as the running mass taken at the scale equal to the mass value itself, i.e. at that μ at which $\mu = m(\mu)$. Even in the multi-generation case when the mass matrix does not rotate but its eigenvalues run with changing scales, one can still define the mass m_i and the state vector \mathbf{v}_i of the state i , as respectively just the i th eigenvalue and eigenvector of the matrix m taken at the scale $\mu_i = m_i(\mu_i)$, with $m_i(\mu)$ being the scale-dependent i th eigenvalue of the matrix m . One might therefore be tempted to suggest the same definitions in the multi-generation case even when the mass matrix rotates. However, this will not do, because it would mean that the state vectors for the different generations i will be defined as eigenvectors of the matrix m at different scales. Although the eigenvectors i for different eigenvalues i are orthogonal, m being hermitian, when taken all at the same scale, they need not be mutually orthogonal when taken each at a different scale. But the state vectors for different flavour states ought to be orthogonal to one another if they are to be independent quantum states. Otherwise, it would mean physically that the flavour states would have nonzero components in each other and be thus freely convertible into one another, or that the mixing matrices would no longer be unitary, which would of course be unphysical.

How then should the mass values and state vectors of flavour states be defined in the scenario when the mass matrix rotates? To see how this question may be resolved, let us examine it anew with first the U type quarks as example. The 3×3 mass matrix m has 3 eigenvalues with the highest value m_1 corresponding to the eigenvector \mathbf{v}_1 , both depending on scale μ . Starting from a high scale and running down, one reaches at some stage $\mu_1 = m_1(\mu_1)$, i.e. when the scale equals the highest eigenvalue m_1 . One can then naturally define this value $m_1(\mu_1)$ as the t quark mass m_t and the corresponding eigenvector $\mathbf{v}_1(\mu_1)$ as the t state vector \mathbf{v}_t . Next, how should

one define the mass m_c and the state vector \mathbf{v}_c ? We have already seen above that they cannot be defined as respectively the second highest eigenvalue m_2 of the 3×3 mass matrix m and its corresponding eigenvector at the scale $\mu_2 = m_2(\mu_2)$, because this vector is in general not orthogonal to the state vector \mathbf{v}_t which the state vector \mathbf{v}_c ought to be. It is not difficult, however, to see what is amiss. At scales below the t mass, i.e. when $\mu < m_t$, t would no longer exist as a physical state, so that what functions there as the fermion mass matrix is not the 3×3 matrix m but only the 2×2 submatrix, say \hat{m} , of m in the subspace orthogonal to \mathbf{v}_t . Hence, for consistency, one should define m_c as the highest eigenvalue \hat{m}_2 of the submatrix \hat{m} and the state vector \mathbf{v}_c as the corresponding eigenvector, both at the scale $\hat{\mu}_2 = \hat{m}_2(\hat{\mu}_2)$. The state vector of c so obtained is automatically orthogonal to \mathbf{v}_t as it should be. Repeating the argument, one defines further the mass m_u and state vector \mathbf{v}_u respectively as the “eigenvalue” and “eigenvector” of \hat{m} at the scale $\hat{\mu}_3 = \hat{m}_3(\hat{\mu}_3)$, with \hat{m} being the 1×1 submatrix of m in the subspace orthogonal to both \mathbf{v}_t and \mathbf{v}_c . Proceeding in this way, all masses and state vectors are defined at their own proper mass scale and the state vectors are mutually orthogonal as they should be. Besides, though stated above only for 3, the definition can be extended to any number of fermion generations, should there be physical incentive for doing so.

Having now made clear the general procedure for defining masses and state vectors for a rotating mass matrix, let us return to consider in particular the implications in the DSM scenario. There, we recall in (3.25) that the mass matrix is of a factorized form:

$$m = m_T |\mathbf{r}\rangle \langle \mathbf{r}|, \quad (4.10)$$

given in terms of a single vector $\mathbf{r} = (x', y', z')$ which rotates with changing scales and in which the whole content of the rotating mass matrix is encapsulated. Since our discussion depends only on the orientation of this vector, the length of which cannot in any case at present be calculated perturbatively, we shall henceforth take \mathbf{r} to be a normalized vector. This mass matrix m is of rank 1 and is aligned to a good approximation for all fermion species. Nevertheless, we claim that because \mathbf{r} rotates with changing scale, we would obtain nonzero masses for the lower generations as well as nontrivial mixing as a result. This is most easily seen by first considering the 2 heavier generations. The procedure of the preceding paragraph gives the state vector \mathbf{v}_t of t as the single massive eigenstate \mathbf{r} of the U quark mass matrix at the scale $\mu = m_t$. As the scale lowers to $\mu = m_c$, the vector \mathbf{r} will have rotated to a different direction as depicted in Figure 5. The state vector \mathbf{v}_c is thus by

definition the vector orthogonal to \mathbf{v}_t lying on the plane spanned by \mathbf{v}_t and $\mathbf{r}(m_c)$. The c mass m_c is then given as the eigenvalue of \hat{m} at scale $\mu = m_c$, which for the rank 1 matrix m in (4.10) is just the expectation value of m in the state \mathbf{v}_c . Hence c acquires by “leakage” a nonzero mass:

$$m_c = \langle \mathbf{v}_c | m | \mathbf{v}_c \rangle = m_t |\langle \mathbf{v}_c | \mathbf{r} \rangle|^2 = m_t \sin^2 \theta_{tc}, \quad (4.11)$$

with θ_{tc} the rotation angle between the scales $\mu = m_t$ and $\mu = m_c$.

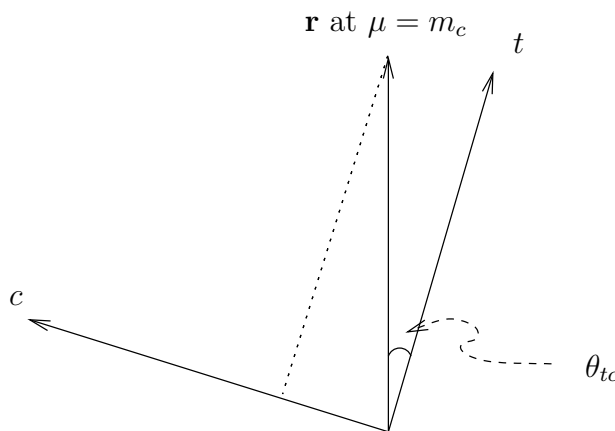


Figure 5: Masses for lower generation fermions from a rotating mass matrix via the “leakage” mechanism.

Similarly, although the mass matrices of the U and D quarks according to (3.25) are always aligned in orientation when both are at the same scale, the state vectors \mathbf{v}_t and \mathbf{v}_b are defined as the vector \mathbf{r} at different scales, namely $\mathbf{v}_t = \mathbf{r}$ at $\mu = m_t$, but $\mathbf{v}_b = \mathbf{r}$ at $\mu = m_b$. Hence, one sees from Figure 6 that simply by virtue of the rotation of the vector \mathbf{r} from the scale $\mu = m_t$ to the scale $\mu = m_b$, a nonzero mixing between the t and b states results with the CKM matrix element given by (4.9) as:

$$V_{tb} = \mathbf{v}_t \cdot \mathbf{v}_b = \cos \theta_{tb}, \quad (4.12)$$

where θ_{tb} is the rotation angle between the two scales.

Hence, already from these examples, one sees that both lower generation masses and nontrivial mixing will automatically be obtained from the rotating mass matrix (3.11) even if one starts with neither. Similar procedures apply to the lowest generation.

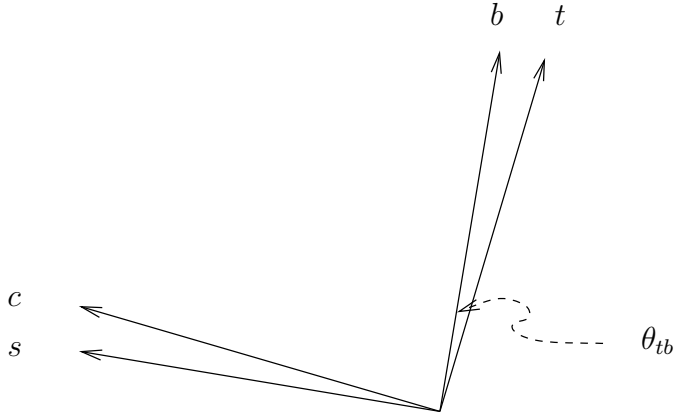


Figure 6: Mixing between up and down fermions from a rotating mass matrix.

We conclude therefore that in spite of its simplicity the renormalized mass matrix of (3.25) is capable by virtue of the rotation induced by equation (3.26) of yielding nonzero masses for the lower generations as well as nontrivial mixing between up and down fermion states. The next question then is whether it can give mass and mixing parameters to agree in value with those observed in experiment. Given the formalism already set up above, it is in principle just a matter to be answered by performing the suggested calculation, which has already been performed at the 1-loop level and will be described in the next section. However, before we do so, it is worth examining the equations to familiarize ourselves with those features which assure us of some reasonable answers. Although we ourselves learned to appreciate these only in hindsight after performing the said calculations in detail, our job would have been much easier had we realised them before.

To see this, let us examine the equation (3.26) in a little more detail. We note first from (3.27) that the two points where (x', y', z') equals $(1, 0, 0)$ or $\frac{1}{\sqrt{3}}(1, 1, 1)$ are rotational fixed points for the vector. Secondly, from (3.26) we see that as the scale μ decreases, the vector $\mathbf{r} = (x', y', z')$ moves away from the point $(1, 0, 0)$ towards the point $\frac{1}{\sqrt{3}}(1, 1, 1)$. In other words, starting say at high scale, as the scale μ lowers, the vector \mathbf{r} traces out a trajectory on the unit sphere joining the high energy fixed point $(1, 0, 0)$ to the low energy fixed point $\frac{1}{\sqrt{3}}(1, 1, 1)$.

Near either fixed point, the rotation will of course be slower, and since according to our previous discussion, both the leakage of masses to the lower generations and the mixing between up and down states come in this scheme

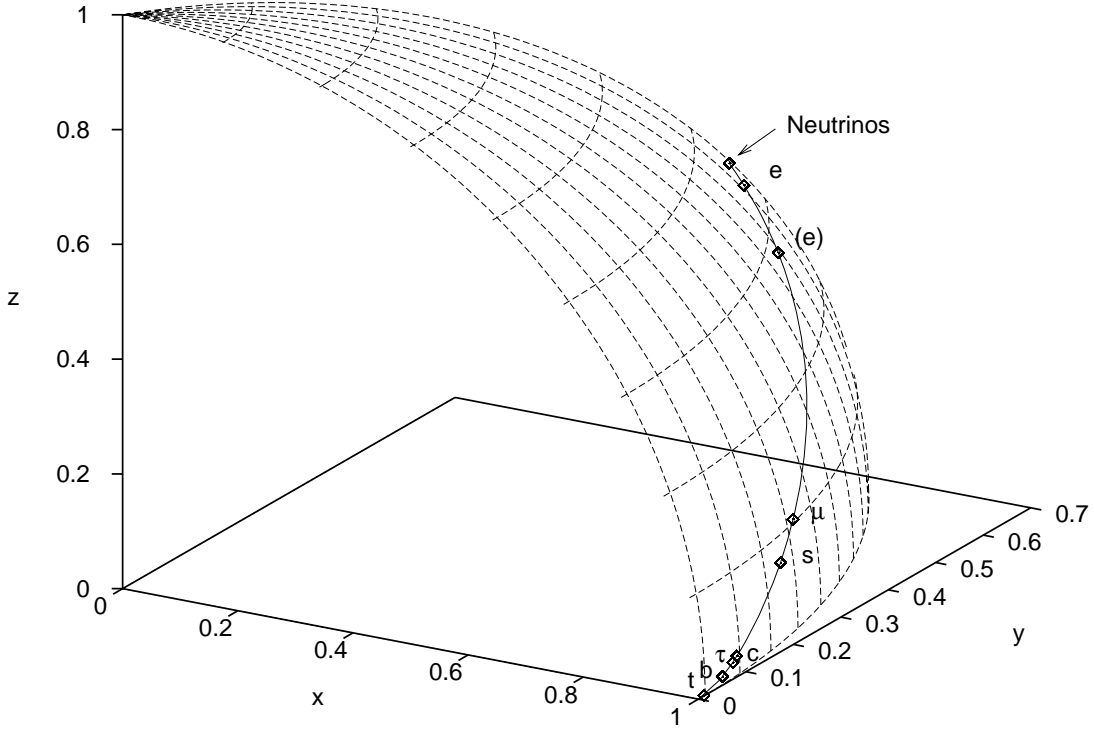


Figure 7: Rotation trajectory of the vector $\mathbf{r} = (x', y', z')$ on the unit sphere as calculated in the 1-loop approximation of DSM in [31]. The locations of the various fermions states marked on the trajectory represent their mass scales, thus for example, the location of t is given by the scale $\mu = m_t = 175$ GeV. For the electron, we have marked 2 locations with e corresponding to $\mu = 0.51$ MeV, the empirical mass of the electron, and (e) to $\mu = 6$ MeV, the calculated mass in the 1-loop approximation. For all the other fermions marked except for the neutrinos, no such distinction is needed since the empirical mass and the calculated mass coincide. For neutrinos, the masses are so small and so close to the low energy fixed point $\frac{1}{\sqrt{3}}(1, 1, 1)$ as to be indistinguishable in the figure. From the marked locations of the various fermion states, one can gauge the rotation speed of \mathbf{r} with respect to change in scale μ . In particular, one notes that rotation is slow near either of the 2 fixed points.

from the rotation, so both these effects will also be smaller at scales near the two fixed points. Suppose therefore we were to choose the parameters of the scheme so as to place the t quark close to the high energy fixed point $(1, 0, 0)$ but the neutrinos close to the low energy fixed point $\frac{1}{\sqrt{3}}(1, 1, 1)$ as indicated in Figure 7. (The trajectory in this figure is actually the result of a calculation to be described later, but will serve as an illustration here.) Then we would be able immediately to deduce the following consequences.

(i) Since t is nearer than b to the fixed point $(1, 0, 0)$, and b is nearer than τ , the mass leakage will also go in that order, namely: $m_c/m_t < m_s/m_b < m_\mu/m_\tau$, which agrees with the experimental values quoted in (1.1).

(ii) Since the neutrinos are much further on the trajectory from the charged leptons than the D quarks are from the U quarks, mixing angles are much larger for leptons than for quarks. This is again as seen in experiment as quoted in (1.2) and (1.3).

(iii) With a bit more sophistication, using some elementary differential geometry [35], it can be shown that the mixing matrices can be approximately expressed in the form [36]:

$$\begin{pmatrix} 1 & -\kappa_g \Delta s & -\tau_g \Delta s \\ \kappa_g \Delta s & 1 & \kappa_n \Delta s \\ \tau_g \Delta s & -\kappa_n \Delta s & 1 \end{pmatrix} \quad (4.13)$$

to first order in the arc-length Δs separating the heaviest up state from the heaviest down state, where κ_g is the geodesic curvature, κ_n the normal curvature, and τ_g the geodesic torsion of the trajectory on a surface. When the surface is the unit sphere, as in our case, $\tau_g = 0$ and $\kappa_n = 1$. This means first that the corner elements of the mixing matrices, i.e. V_{ub} and V_{td} of CKM, and U_{e3} of MNS, must be much smaller than the other elements, which is seen to be the case in (1.2) and (1.3). Secondly, the 23 element is proportional roughly to the separation Δs , which explains why the mixing angle $U_{\mu 3}$ for atmospheric neutrinos is so much bigger than the corresponding angle V_{cb}, V_{ts} for quarks, an experimental observation which has caused much recent excitement.

Thus, even without a detailed calculation, one can already see that there is a good chance of obtaining qualitatively reasonable result from the present scheme for fermion mass and mixing parameters. The only question is really whether one can choose the few parameters inherent in the scheme to explain sufficiently the existing data. This will be decided by explicit calculations, which form the subject of the next section.

Before we do so, however, we notice that in our above discussion from equation (4.10) onwards, we have taken the vector \mathbf{r} factored from the mass matrix to be a real vector to conform with what was obtained from the DSM 1-loop calculation begun in the preceding section and continued in the next. This means that the CKM and MNS matrices which result are both going to be real and can give no CP-violation. But this is a limitation only of the 1-loop calculation, not of the general considerations in this section which can be repeated virtually unchanged with \mathbf{r} complex, thus accounting for a CP-violating phase, as might become necessary, for example, when higher loop effects are involved.

5 1-loop DSM Result on Masses and Mixing Angles

The subject of this section is the calculation of the rotating fermion mass matrix to 1-loop order with the initial object of explaining the mass and mixing patterns of quarks and leptons as experimentally observed. Since the parameters of the problem have yet to be determined by fitting with data, the question of applicability and accuracy of the 1-loop approximation, and if so in what physical range, can in principle only be answered after the calculation has been performed, and then only to the limit of our understanding. However, anticipating our results, to a discussion of which we shall return at the end, we suggest that the calculation can be expected generally to be valid to a rough accuracy of say 20 to 30 percent in mass ratios and mixing parameters over a range of energy scales starting from about the top mass at 175 GeV down to about the muon mass at 105 MeV. As we shall see, however, there are special circumstances which allow us to expect reasonable accuracy also for some other quantities such as the elements U_{e3} and $U_{\mu3}$ of the lepton mixing matrix associated with neutrino oscillations, although these lie formally outside the above scale range. These conclusions have much to do with the existence of the two rotational fixed points mentioned above at respectively infinite and zero scales, near to which the 1-loop approximation has a better chance of being valid.

Even to 1-loop order, of course, there are in principle many diagrams which can contribute to the renormalization of the fermion mass matrix. However, if we accept the contention made above, that mass “leakages” and mixings of fermions are due mainly to mass matrix rotations, then the problem simplifies tremendously [28]. First of all, the insertions of the type

present already in the conventional formulation of the Standard Model, not being directly dependent on dual colour (i.e. the generation index) contribute practically nothing to the rotation of the fermion mass matrix. Secondly, of the new diagrams involving the exchange of gauge and Higgs bosons carrying dual colour or generation index which are listed together in Figure 8, all except the Higgs loop insertion already calculated give rotations only of order μ^2/M^2 , with M of order 100 TeV, and are therefore negligible for the effects we seek. This is very fortunate, for it means that to 1-loop order, the result already calculated and qualitatively analysed in the preceding 2 sections is all that we would need.

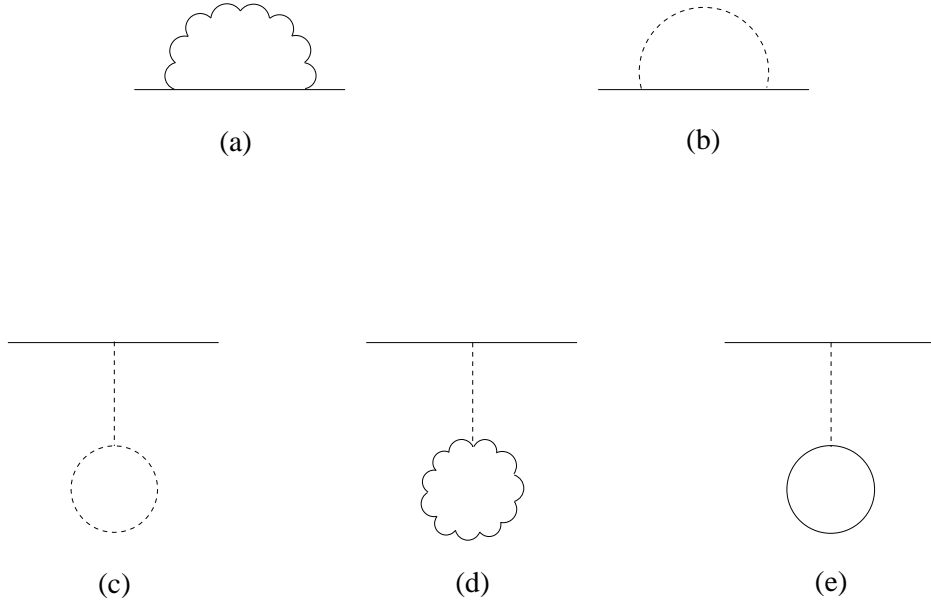


Figure 8: One-loop diagrams with gauge and Higgs bosons carrying dual colour.

To the accuracy we need, then, the fermion mass matrix to 1-loop order is given by (3.25) in terms of a vector $\mathbf{r} = (x', y', z')$ in 3-dimensional generation space which rotates with changing scale according to the evolution equation (3.26). Referring back to (3.26) and (3.27), one sees that apart from a mass

scale m_T for each fermion species, the remaining freedom is only in the choice of trajectory for the vector \mathbf{r} , and the Yukawa coupling strength ρ which governs the speed of the vector's rotation along the trajectory. The vector being by definition a unit vector, the trajectory will be specified by a choice of some initial values, say y_I, z_I of y', z' . The coupling ρ could, as mentioned already, depend on the fermion species, but for consistency with the present interpretation have to be the same for all. This can be seen either numerically as shown in [28] or else analytically from an approximate solution of the evolution equation [32]. One has then altogether just 3 real parameters to explain the mass ratios between generations and the mixing matrices between up and down states for both quarks and leptons.

The equation (3.26), being linear, is easily integrated for any given value of the coupling parameter ρ and any initial point on the trajectory, say (x_I, y_I, z_I) , at any chosen scale μ_I . The integration can be done numerically by iteration as in [28, 31], where for the 1 percent accuracy aimed for which would be more than adequate for present purposes, roughly 500 steps of iteration are made per decade change in energy, the vector $\mathbf{r} = (x', y', z')$ being re-normalized to unit length after every step. Having obtained then the trajectory, i.e. the vector \mathbf{r} at every scale, it is an easy matter, following the procedure described in the above section, and given the normalization m_T of the mass matrices, to calculate the mass ratios between generations for each of the 4 fermion species $T = U, D, L, N$, as well as the elements of both the CKM and MNS mixing matrix for quarks and leptons respectively. However, although for the up and down quarks and charged leptons, the normalization m_T can be taken respectively as m_t, m_b, m_τ which are all by now quite well measured [1], m_T for neutrinos is still unknown, being given in the above formulation by the Dirac mass of the heaviest state ν_3 (which is most likely distinct from the physical mass because of the see-saw mechanism [33]). Hence, only the numerical values of the mass ratios for $T = U, D, L$ and the CKM mixing matrix for quarks are obtained at this stage. These numbers, however, still depend on the given choice of parameters y_I, z_I and ρ , and need not of course agree with the empirical values. One has thus first to determine the appropriate values of these parameters by fitting to experiment.

For convenience and without loss of generality, we can take $x_I \geq y_I \geq z_I$ at some arbitrary high scale value μ_I which is chosen to be 20 TeV in [28, 31]. The strategy is then to fit the 3 parameters y_I, z_I and ρ to the 3 best measured quantities among the fermion mass and mixing parameters which are at present the mass ratios $m_c/m_t, m_\mu/m_\tau$ and the Cabbibo angle

$V_{us} \sim V_{cd}$. One then varies the parameters and recalculates these 3 quantities with the above procedure until agreement is obtained with the experimental values. A useful point to note is that whereas the mass ratios $m_c/m_t, m_\mu/m_\tau$ depend mostly on the parameters ρ and y_I , which govern respectively the speed of rotation and the curvature of the rotation trajectory, the Cabbibo angle is sensitive to z_I which governs the nonplanarity of the trajectory. The best fit obtained in [31] with the central values given by the Particle Physics Booklet at that time [39] for $m_c/m_t, m_\mu/m_\tau$ and the Cabbibo angle gives (see, however, footnote after equation (3.27)):

$$\rho = 4.564, \quad y_I = 0.0017900, \quad z_I = 0.0000179. \quad (5.1)$$

With these fitted parameters in hand, one can now calculate the trajectory to 1-loop level, the result of which is shown in Figure 7. The speed at which the vector $\mathbf{r} = (x', y', z')$ rotates with change in scale μ is not explicitly shown in this figure but can be gauged from the locations on the trajectory of the various quark and lepton states each marked at the scale μ equal to the mass of that particular state. The same result will be presented again later in Figure 10 in which the μ -dependence is made explicit. One notices in Figure 7 that the trajectory calculated with the parameters fitted as above automatically puts the t quark very near the high energy fixed point $(1, 0, 0)$, and the neutrinos bunched up near the low energy fixed point $\frac{1}{\sqrt{3}}(1, 1, 1)$. This means that the qualitative arguments of the last section apply, so that some reasonable values for the mixing angles and mass ratios can already be anticipated. Besides one sees that the rotation, as expected, is slow near the high energy fixed point at $(1, 0, 0)$ so that from $\mu = \infty$ to the scale of the top mass m_t at 175 GeV, the vector \mathbf{r} has rotated only by an angle of about 0.03 radians. Even down to the scale of the muon mass m_μ at 105 MeV, the rotation angle is still of order only 0.3 radians, and that is the reason already mentioned at the beginning of the section why one expects the 1-loop approximation to be still roughly valid down to this energy region, with 2-loop contributions presumably of order of the square of the 1-loop, leading to about a 30 percent correction. The rotation, however, will continue to accelerate as the scale moves further down so that for scales μ less than the muon mass, the above 1-loop approximation will become unreliable. This means in practice that it should normally be applied only to the 2 heavier generations of the U, D, L fermion species and not to neutrinos, except under special circumstances of which there are some very important examples to be explained later.

Having calculated the rotation trajectory of the vector \mathbf{r} and hence of the fermion mass matrix (3.25), one can now follow the prescription detailed in the preceding section to evaluate the masses and state vectors of all the 9 states of the U, D and L fermion species, but with the above proviso that only the results for the 2 heavier generations are normally to be trusted. We note, however, that since in each fermion species the state vectors of the 3 generations form together an orthonormal triad, the state vector of the lightest generation is already determined by the state vectors of the 2 heavier generations which in turn are already determined at the mass scale of the second heaviest state. Hence, despite the proviso above, one concludes that all 3 state vectors can be evaluated with confidence already at the 1-loop level. This is fortunate, for it means for quarks in particular that the triads for both U and D quarks are now determined and this allows one immediately via (4.9) to evaluate the whole CKM matrix (apart from the CP-violating phase as explained above). The result obtained with the parameters in (5.1) is as follows [31]:

$$\begin{pmatrix} |V_{ud}| & |V_{us}| & |V_{ub}| \\ |V_{cd}| & |V_{cs}| & |V_{cb}| \\ |V_{td}| & |V_{ts}| & |V_{tb}| \end{pmatrix} = \begin{pmatrix} 0.9745 - 0.9762 & 0.217 - 0.224 & 0.0043 - 0.0046 \\ 0.217 - 0.224 & 0.9733 - 0.9756 & 0.0354 - 0.0508 \\ 0.0120 - 0.0157 & 0.0336 - 0.0486 & 0.9988 - 0.9994 \end{pmatrix}, \quad (5.2)$$

where the range of values in the entries represent the spread in values given by the data booklet for the fitted quantities $m_c/m_t, m_\mu/m_\tau$ and the Cabibbo angle. It is seen that (5.2) not only shares the general features noted in the empirical CKM matrix (1.2) as expected already by the qualitative considerations in the preceding section, but even agrees quantitatively with the empirical CKM matrix all to within the quoted experimental errors.

By the same token as for quarks, the above 1-loop calculation for the rotation trajectory for the vector \mathbf{r} should give the state vectors of the 3 charged leptons τ, μ, e with some confidence. Explicitly, one obtains [31]:

$$\begin{aligned} |\tau\rangle &= (0.996732, 0.076223, 0.026756), \\ |\mu\rangle &= (-0.075925, 0.774100, 0.628494), \\ |e\rangle &= (0.027068, -0.628482, 0.777354). \end{aligned} \quad (5.3)$$

However, these by themselves do not allow one to calculate the MNS mixing matrix, for which one will need also the state vectors of the neutrinos. The

present empirical bound on the mass of the electron neutrino from e.g. tritium decay experiments is of order eV, which in turn implies that the mass differences of the heavier neutrinos ν_2 and ν_3 are restricted by neutrino oscillation experiments to order 0.1 eV or less. This puts all active neutrinos in the eV mass scale range or lower, which is clearly way beyond the range of validity of the above 1-loop calculation. Once again, however, there are fortunate special circumstances here that help us through [32]. According to the prescription of the preceding section, the state vector of the heaviest neutrino ν_3 , as for the heaviest generation in all other fermion species, is just the vector \mathbf{r} taken at the mass scale of ν_3 , i.e. at eV scale or lower. According to Figure 7, however, the vector \mathbf{r} at the eV scale would already be very close to the low energy fixed point at $\frac{1}{\sqrt{3}}(1, 1, 1)$ and can be well approximated by it, thus:

$$|\nu_3\rangle \sim \frac{1}{\sqrt{3}}(1, 1, 1). \quad (5.4)$$

So applying the formula (4.9) for mixing matrix elements with the help of (5.3) above gives immediately:

$$\begin{aligned} U_{\mu 3} &= \langle \mu | \nu_3 \rangle = 0.7660, \\ U_{e 3} &= \langle e | \nu_3 \rangle = 0.1016. \end{aligned} \quad (5.5)$$

Again, one sees that these results agree with present data (1.3) within the experimental errors. That the mixing element $U_{\mu 3}$ should be large and $U_{e 3}$ small was expected already from the qualitative considerations of the preceding section with elementary differential geometry. That $U_{\mu 3}$ should turn out, however, to be near maximal in agreement with oscillation experiments on atmospheric neutrinos [5, 6], and that the CHOOZ angle to be within the experimental bounds [11], are particular achievements of the 1-loop calculation above.

The mass of ν_2 , being by definition even lower than that of ν_3 , will be even nearer the low energy fixed point $\frac{1}{\sqrt{3}}(1, 1, 1)$. However, one cannot as yet determine the state vector of ν_2 , which being essentially the tangent vector to the trajectory of \mathbf{r} at the fixed point, will depend more on the actual trajectory, namely on how the trajectory approaches the fixed point. It is thus not expected to be well reproduced by the above 1-loop calculation which will be unreliable at these energies. Indeed, should one persist nevertheless to calculate $|\nu_2\rangle$ and hence the mixing element $U_{e 2}$ as we did in [31] before we had realized clearly the limitations of the 1-loop approximation, one obtains $U_{e 2} = 0.24$ which is largish as solar neutrino experiments show it to be but

lies outside present experimental limits. We shall return later to comment further on this point⁶.

Having now exhausted the consequences of the above 1-loop calculation on the mixing matrices, let us turn next to those on the mass ratios between generations. Here the result is much less conclusive, for several reasons. First, in contrast to the above calculation of the mixing parameters, the calculation of lower generation masses depends on the assumption that the normalization m_T of the mass matrix written in the form (4.10) is roughly constant with changing scale, which may be reasonable over small scale changes, such as that between the 2 heavier generations considered so far, but would be unreliable when larger scale changes are involved as when the lightest states are also taken into account. Secondly, of the 3 measured mass ratios involving only the 2 heavier generations, 2 ratios ($m_c/m_t, m_\mu/m_\tau$) have already been used to fit the parameters of the model, leaving only m_s/m_b which is poorly measured. Although a value for $m_s/m_b = 0.039$ is obtained which is within the wide experimental bounds, no great significance can be given to the agreement. Thirdly, the remaining lightest members of the U, D, L species, namely u, d and e , all lie outside the scale range of applicability of the 1-loop calculation so that its predictions for their masses cannot be trusted. Should one persist as we did in [31], one would obtain for m_e a value of 6 MeV, an order of magnitude off the empirical value 0.5 MeV, which is already not too bad, considering that it is an extrapolation in a logarithmic scale over several orders of magnitude. Again, we shall return later for a comment on this. Fourthly, for the remaining u and d quarks, these have the additional complication of being tightly confined, while the prescription given in the last section for calculating fermion masses applies only to free particles. Indeed, we do not know at present how to calculate the masses of these tightly confined states. The masses of u and d quoted in the data booklets [39, 1] were determined at values of the running scale of 1 and 2 GeV respectively. If we were to define the masses of u and d as the leakage of the vector \mathbf{r} at these scales to respectively the u and d states which we already know, we would obtain masses of the order of MeV, which is of the right order of magnitude. But we are not at all confident that this is the correct

⁶The above treatment of neutrino oscillations to 1-loop level in DSM [32] updates and supercedes our earlier treatment in [38]. The older treatment made additional assumptions on neutrino masses, and applied to only the vacuum oscillation solution for solar neutrinos. The present treatment needs no special assumptions for neutrinos and applies as well to the experimentally favoured large mixing angle (LMA) solution for solar neutrinos, besides accounting properly for the limitations of the 1-loop approximation.

prescription. As for neutrino masses, one has no predictions so far from the above considerations, except that they have in general nonzero masses.

To summarize, with 3 parameters fitted to experiment, one has calculated to 1-loop approximation the rotation trajectory which allows one then to determine the mixing matrices and mass ratios between generations. Having now explored all possibilities, one finds agreement with data to within experimental errors for all quantities which are inside the estimated range of applicability of the 1-loop approximation. These include all 9 elements of the CKM matrix $|V_{rs}|$, $r = u, c, t$, $s = d, s, b$, the 2 elements $|U_{\mu 3}|$, $|U_{e 3}|$ of the MNS matrix, as well as the 3 mass ratios $m_c/m_t, m_s/m_b, m_\mu/m_\tau$, and together account for 8 of the 25 or so independent “fundamental” parameters of the Standard Model as usually formulated. For the remaining quantities which lie outside the range of applicability of the 1-loop approximation, namely $|U_{e 2}|, m_e, m_u, m_d$, if one persists nevertheless with the 1-loop approximation, one obtains sensible values of roughly the right order as expected already from our previous qualitative considerations but lying outside experimental bounds. In other words, apart from the one important piece of the puzzle of CP-violation of which one has still found no trace, the DSM scheme taken to the 1-loop level seems at present to be in the happy position of having been shown to be right in all cases where it is expected to be right and to have only qualitative but not quantitative agreement with data in circumstances where the 1-loop approximation made is expected to be unreliable [32].

The above result has one perhaps unexpected aspect in that the rotation effect crucial for its derivation is obtained from 1-loop diagrams with heavy dual colour Higgs boson exchanged where normally one would expect that at the low energies one is dealing with the heavy bosons could be integrated out and largely ignored. We think, however, that there are special circumstances here which differ from the normal expectation. Given the initial assumption that these bosons exist, then they will in any case contribute at 1-loop to the renormalization of the fermion mass matrix as calculated. The terms proportional to $\ln \mu$ which affect the rotation occur as wave function renormalization and are not among those shown by Appelqvist and Carrazone to be of order s/M^2 in their decoupling theorem [40]. Nevertheless, one might have expected them to be overwhelmed at low energy scales both by the higher loop contributions of these heavy bosons, and by the loop diagrams of the Standard Model particles, such as gluons and electroweak gauge and Higgs bosons. However, as already mentioned, in the special case of mass matrix rotation that we are looking at, the higher loop corrections due to

dual colour bosons are small because of the proximity to the rotational fixed points in the scale regions under consideration, while, even more importantly, the contributions of the Standard Model particles to the rotation give zero. For this reason, it appears that for lack of competition, the 1-loop contribution of the heavy bosons will still dominate and give already a reasonable approximation. However, without a more detailed investigation, one cannot go any further than this qualitative observation, and can at present only leave the positive results to speak for themselves.

The conclusion of general agreement with data, however, holds at this moment only as regards the fermion mass and mixing patterns, which are the only pieces of data so far explored. Consequences in other areas have yet to be examined later in section 7. Besides, the success of the predictions, of course, need by no means imply that the whole chain of arguments leading to the predictions are correct. Our next task therefore is to examine which of the arguments are essential and which are not for obtaining the above positive result.

6 Direct Empirical Support for Mass Matrix Rotation

The DSM 1-loop calculation reported above giving good agreement with experiment on fermion mass and mixing parameters was first performed numerically [28, 31] but has since been checked by analytic calculations under certain approximations [32], and being backed up further by the qualitative considerations of section 4, seems unlikely to be pure coincidence. What is unclear, however, is whether the apparent success can be ascribed to the assumptions that have been made, and if so to what extent and to which of them. In other words, we wish to ask what the above calculation has actually taught us about the underlying physics.

It has already been pointed out in [31] that although the concept of non-abelian duality as described in section 2 and the identification of the dual colour symmetry with the horizontal symmetry of generations are seminal in first of all offering a geometric explanation for the existence of 3 fermion generations, and secondly in suggesting a new framework for calculating the fermion mass hierarchy and mixing phenomena, they are not absolutely essential for obtaining the desired result. Indeed, neither the Higgs potential (3.4) nor the Yukawa coupling term (3.8) from which the calculation develops have been shown to follow logically from nonabelian duality, and so long as

one has a horizontal symmetry with these two ingredients, the same calculation can be carried through with the same apparent success without any reference to nonabelian duality or to its identification with generations. Furthermore, as far as the qualitative features of the fermion mass hierarchy and mixing are concerned, it would appear from the discussion of section 4 that what is really crucial is that the mass matrix should rotate and that there should be rotational fixed points at infinite and zero energy scales. Where the suggested Higgs potential and Yukawa coupling come in is really only in supplying the detailed fit to the experimental numbers. Superficially at least, it would seem conceivable that given a rotation trajectory depending on several parameters, so long as it has the same rotational fixed points as above, then very similar results would obtain, regardless of the theoretical premises from which the rotation trajectory may arise.

One can go even further and ask whether the rotation itself is necessary. To answer this question, one can proceed as follows, namely by turning the problem around and discarding at first even the assumption of a rotational trajectory but seeking instead evidence for it directly from experimental data. This seems at first sight a tall order, but turns out actually to be practicable under certain assumptions as we shall now explain. From the discussion in section 4, one sees that so long as the mass matrix, for whatever reason, can have different orientations at different energy scales, then the usual definition of fermion masses and state vectors will have already to be refined. In particular, even a rank 1 mass matrix (i.e. with only one nonzero eigenvalue) will acquire nonzero masses for the 2 lower generations, and even when the mass matrices of up and down fermions are aligned in orientation at the same scale, there will be nontrivial mixing between them when the difference in orientation at different scales is taken into account. And these effects are immediately calculable once the difference in orientation of the mass matrix at different scales is known. Suppose then we assume that all masses for the 2 lower generations as well as the mixing between up and down states arise only from this effect, we can then turn the argument around and ask what differences in orientations are necessary at different scales to produce the experimentally observed mass ratios and mixings. When this information is extracted from the data and plotted as a function of the scale, then if the hypothesis of a rotational trajectory is indeed correct, the data points will not be randomly scattered but should all lie on some smooth curve. And if they do, one will then have evidence for the rotational trajectory directly from experimental data.

To see practically how this can be done, let us first work in the simplified

scenario with only the 2 heavier generations in each fermion species, which will bring out many of the salient points in a transparent manner. Besides, it will be seen to be already a good approximation for the high mass scale region. The problem now being planar, the difference in orientation of a vector between 2 scales is given by an angle which is additive in the sense that the difference θ_{13} from scale 1 to scale 3 equals the sum $\theta_{12} + \theta_{23}$ of the difference from scale 1 to scale 2 and that from scale 2 to scale 3. As explained above, we start with a rank 1 mass matrix (in the hermitian Weinberg notation), which is thus necessarily of the factorizable form (4.10) given in terms of a single vector \mathbf{r} and it is the dependence of this vector on the energy scale we wish to trace, using experimental data on mass ratios and mixing matrix elements. Consider first the mass ratio m_c/m_t with $m_t = 174.3 \pm 5.1$ GeV and $m_c = 1.15 - 1.35$ GeV as given in [1]. By (4.11) this is just $\sin^2 \theta_{tc}$, from which one easily extracts the value of θ_{tc} together with the appropriate errors. Similarly, using (4.12) one extracts again easily from the value of the CKM matrix element $|V_{tb}|$ the value of θ_{tb} . The same can be done for all other pieces of data involving the 2 heavier generations in the U, D, L fermion species to deduce the differences in orientation between the different mass scales. The result [41] is plotted in Figure 9, where one has made use of additivity to deduce, for example, that $\theta_{ts} = \theta_{tb} + \theta_{bs}$, with θ_{tb} already obtained from $|V_{tb}|$ above, and θ_{bs} from the mass ratio m_s/m_b [39, 1]. One sees in the figure that the extracted data points all lie comfortably on a smooth curve, which can thus be regarded as empirical evidence for rotation, i.e. for the vector \mathbf{r} tracing out a trajectory as the scale changes. Indeed, the trajectory traced out by the data is surprisingly close to that calculated in [31] several years before the data were examined in this way. A best fit with MINUIT to the data points in Figure 9 gives the dotted curve shown which is seen to be hardly distinguishable from the full curve obtained from the calculation in [31].

The evidence cited above for the rotation hypothesis based on Figure 9 is subject to the planar approximation which takes into account only the 2 heavier generations in each fermion species. However, it can be seen that for the numbers so far extracted the approximation is already sufficiently accurate. Take for example the angle θ_{ts} which was extracted above using additivity based on the assumption that the 3 vectors \mathbf{r} at the 3 mass scales of t, b and s all lie on the same plane, which is of course not exact. Indeed, the deviation from planarity is given by the Cabbibo angle, i.e. the angle between the state vectors of the u and d quarks which are respectively normal to the planes spanned by the state vectors of t and c and those of b and s . From the

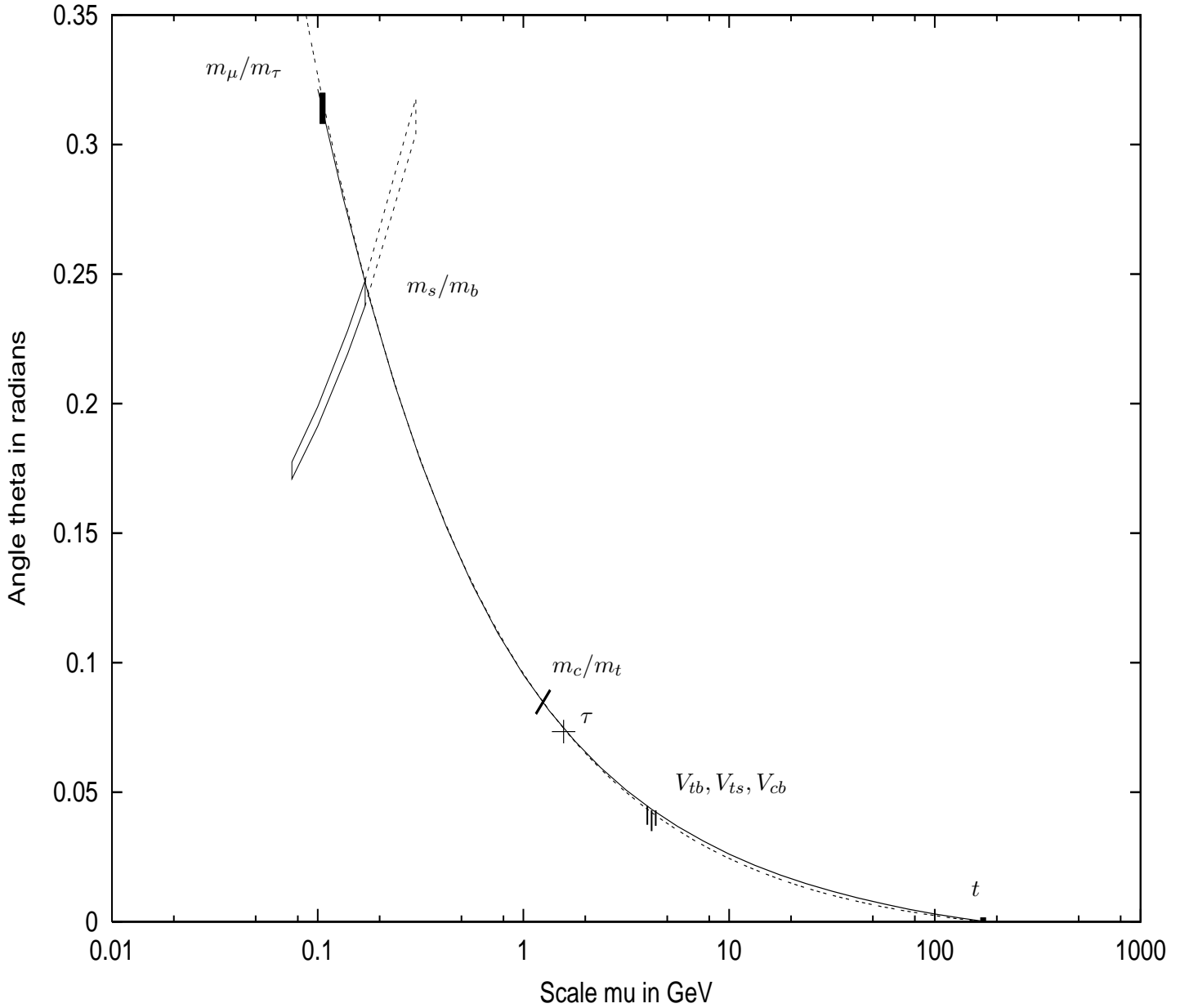


Figure 9: The rotation angle changing with scale as extracted from data on mass ratios and mixing angles (in the “planar” approximation with only the 2 heavier generations) and compared with the best fit to the data with an exponential (dashed curve) and the earlier calculation by DSM (full curve) [31].

empirical value of the Cabbibo angle of around 0.22 radians and the fact that all the angles exhibited in the Figure 9 depend on the square of the Cabbibo angle, one estimates that the error committed by the planar approximation is of order of only 4 percent and hence does not affect the significance of the evidence for rotation claimed above.

The planar approximation, however, worsens as the scale lowers further and cannot therefore be used to extend the analyses to the electron and neutrinos regions which are of crucial physical interest. Besides, it does not reveal the details in the off-planar direction which could in principle contain surprises upsetting the above positive result. For this reason, a full 3 generation repeat of the above analysis is necessary in order to draw a firm conclusion. Since the mass matrix is of rank 1 by our initial assumption, it is still factorizable in terms of a single vector \mathbf{r} which changes orientation with changing scale. And to extract the variations of this vector between different mass scales is no different in principle for 3 generations than for 2, only in practice more complicated. There are more angles involved and simple additivity no longer applies, but with patience the analysis can be carried through. Take, for example, the interesting case of the vector \mathbf{r} taken at the mass scale of the heaviest neutrino ν_3 . The MNS mixing matrix elements $|U_{\mu 3}|$ and $|U_{e 3}|$ are now constrained by oscillation experiments with respectively atmospheric [5, 6] and terrestrial neutrinos [11, 42] to within the following bounds: $1/3 < |U_{\mu 3}|^2 < 2/3$ and $|U_{e 3}|^2 < 0.027$. Now (4.9) gives $|U_{\mu 3}| = \langle \mu | \nu_3 \rangle$ and $|U_{e 3}| = \langle e | \nu_3 \rangle$. Hence, if the state vectors $|\mu\rangle, |e\rangle$ are exactly known as well as the quantities $|U_{\mu 3}|, |U_{e 3}|$, then the state vector $|\nu_3\rangle$ is determined up to discrete sign ambiguities. Even as matters stand, where the quantities involved are known only within certain experimental bounds, it still means that the state vector of ν_3 will be constrained within well defined limits, which can then be checked for consistency with the rotation hypothesis. Furthermore, we recall from our earlier discussion that $|\nu_3\rangle$ is supposed to have almost reached the asymptotic limit of the fixed point at zero scale predicted by the DSM, which prediction could also thus be directly confronted with the limits extracted from data.

In any case, the full 3 generation analysis has been carried out tracing the trajectory of \mathbf{r} over some 14 orders of magnitude in energy scale from the mass scale of the top quark to that of the second heaviest neutrino ν_2 with the result shown in Figure 10. The technical details involved can be found in [41]. Figure 10 gives in a 3-dimensional plot the second and third components of the vector \mathbf{r} extracted from the data for various scales corresponding to the masses of the fermions states. For technical reasons,

these are given in a frame defined by the U quark triad as frame vectors (i.e. $\mathbf{v}_t = (1, 0, 0)$, $\mathbf{v}_c = (0, 1, 0)$, $\mathbf{v}_u = (0, 0, 1)$), not in the old frame where the high energy fixed point appears as $(1, 0, 0)$. Apart from the information from the masses of u and d which is ambiguous for reasons already explained and that from the solar neutrino angle which cannot easily be presented in this figure (see later, however), the data points shown represent all the information on the vector \mathbf{r} that could at present be extracted from experiment on fermion masses and mixing. And it can be seen in the figure that all these data, instead of being a random collection of points, are perfectly consistent with them lying on a smooth 3-D curve. The consistency can be scrutinised further in the 3 projections of Figure 10 on to the 3 coordinate planes shown in Figures 11, 12, and 13, where it is seen in Figure 11 that even the oscillation data from solar neutrinos missed out in Figure 10 satisfy this consistency, as indicated there by the dotted curve. This overall consistency with the rotation hypothesis seems quite nontrivial especially in the high scale region above the muon mass, given the accuracy of the data there.

The full curve in the Figure 10 and its 3 projections represents the 1-loop result from the DSM calculation of [31] described in section 5. It is seen that above the scale $\mu = m_\mu$ it passes through all the data points within errors. That this is the case was already discussed in the preceding section, but as displayed in these figures together with the experimental errors, it is easier to appreciate the significance of the surprisingly good agreement between the calculation and experiment. At scales below the muon mass, the 1-loop curve deviates from the data as expected, thus missing the 2 allowed regions for \mathbf{r} deduced respectively from the electron mass and the solar neutrino angle U_{e2} . It would be interesting to enquire, as we are now trying to do, whether a 2-loop calculation would improve the agreement in the low scale range.

Although the DSM scheme has done extremely well in fitting the data with only 3 parameters, one can still wonder whether all of its details are strictly necessary. Given that the vector \mathbf{r} extracted directly from the data already seems to trace out a rotation trajectory, it would appear that, as described in section 4, if one used a rotating mass matrix of rank 1 having fixed points at infinite and zero scales, then with several adjustable parameters to fit the rotational trajectory, one could probably already manage quite well phenomenologically without appealing to the other details. We take this to mean that minor modifications of the DSM scheme as it now stands, which might in future be found necessary for theoretical reasons, could well leave intact the phenomenological successes so far achieved. What we have in mind is the possibility that a closer examination of duality may lead to some unique

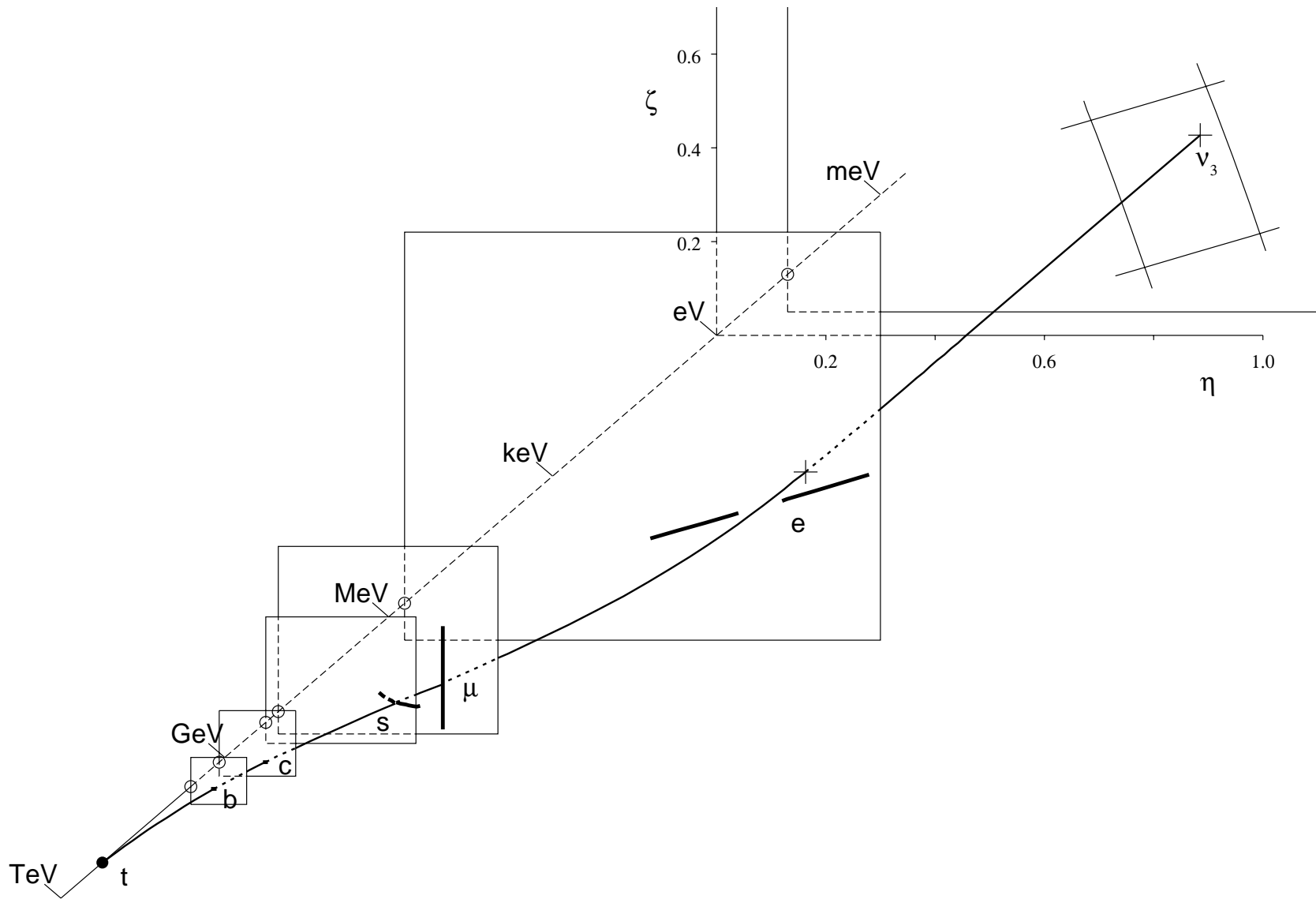


Figure 10: A plot of the rotating vector $\mathbf{r}(\mu)$ as extracted from existing data on fermion mass ratios and mixing parameters, where its 2nd and 3rd components η and ζ are plotted as functions of $\ln \mu$, μ being the energy scale. The experimentally allowed values at any one scale are represented as an allowed region on a plaquette, with the scale corresponding to a plaquette being given by the intersection, denoted by a small circle, of its left-most boundary with the μ -axis. For example, the first small plaquette on the left of the figure corresponds to the scale $\mu = m_b$, on which plaquette the allowed region for $\mathbf{r}(\mu) = \mathbf{v}_b$ is very small because of the small experimental error on the CKM matrix elements V_{tb} , V_{cb} and V_{ub} . The last plaquette on the right, on the other hand, corresponds to the scale $\mu = m_{\nu_3}$, on which plaquette the allowed region for $\mathbf{r}(\mu)$ is a rough rectangular area bounded by the data on ν oscillations from atmospheric neutrinos and from the Chooz experiment. The curve represents the result of a DSM one-loop calculation from an earlier paper [31] which is seen to pass through the allowed region on every plaquette except that for the electron e . For further explanation of details, please see text.

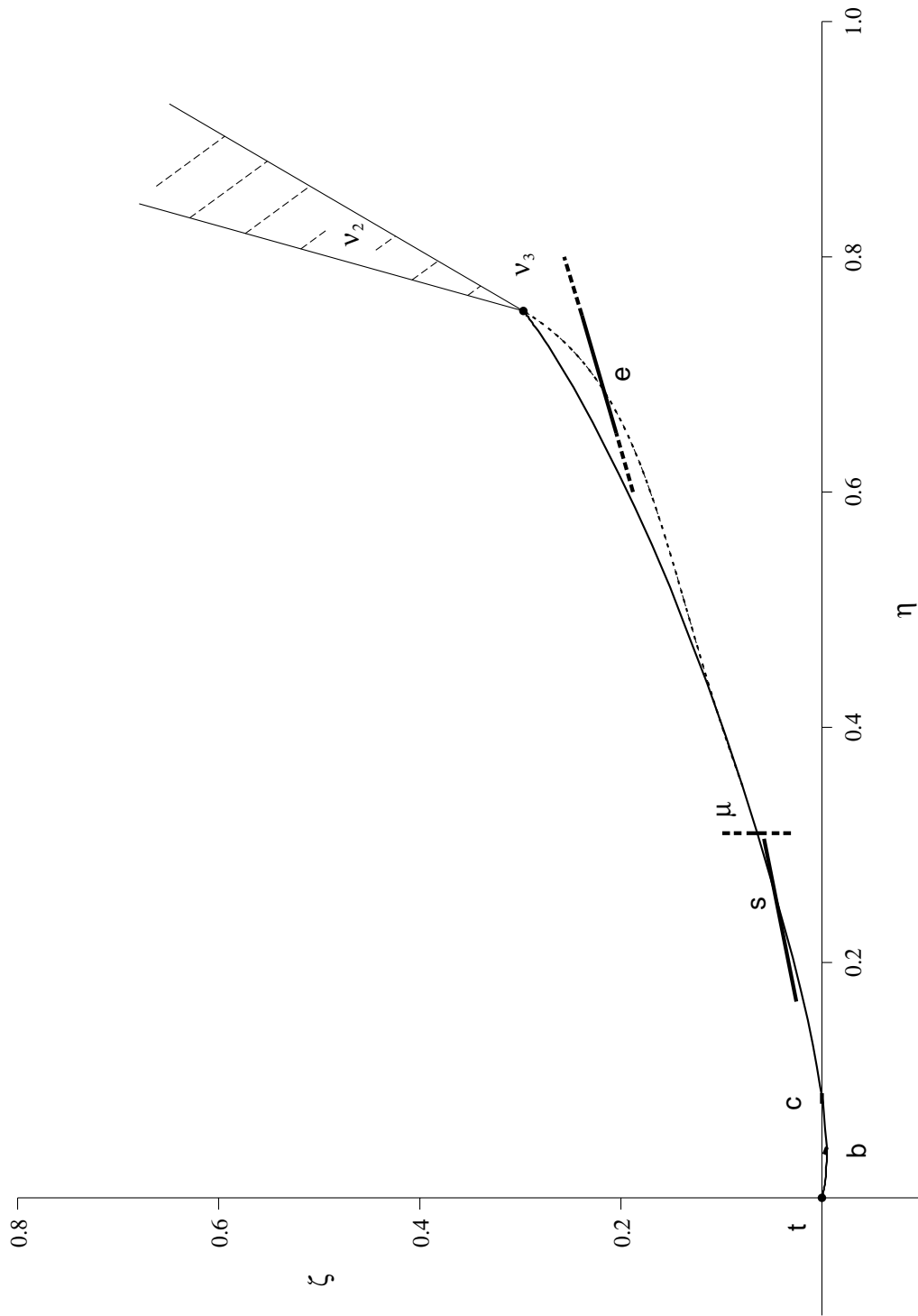


Figure 11: Projection of Figure 10 on to the $\eta\zeta$ -plane. The full curve represents the DSM one-loop calculation of [31] and the dashed curve its suggested deformation at low scales to fit the data on m_e and U_{e2} .

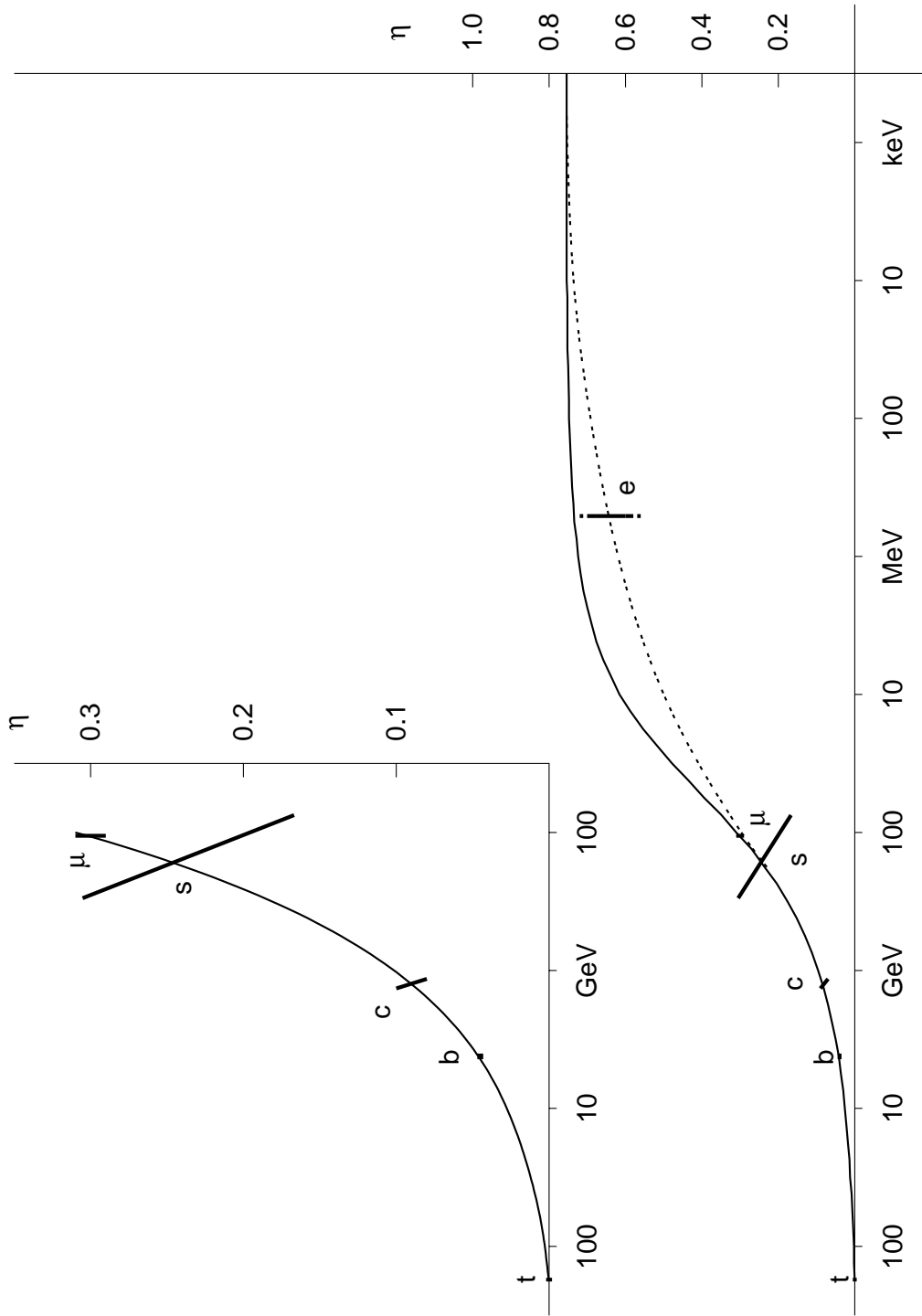


Figure 12: Projection of Figure 10 on to the $\mu\eta$ -plane. The full curve represents the DSM one-loop calculation of [31] and the dashed curve its suggested deformation at low scales to fit the data on m_e and U_{e2} .

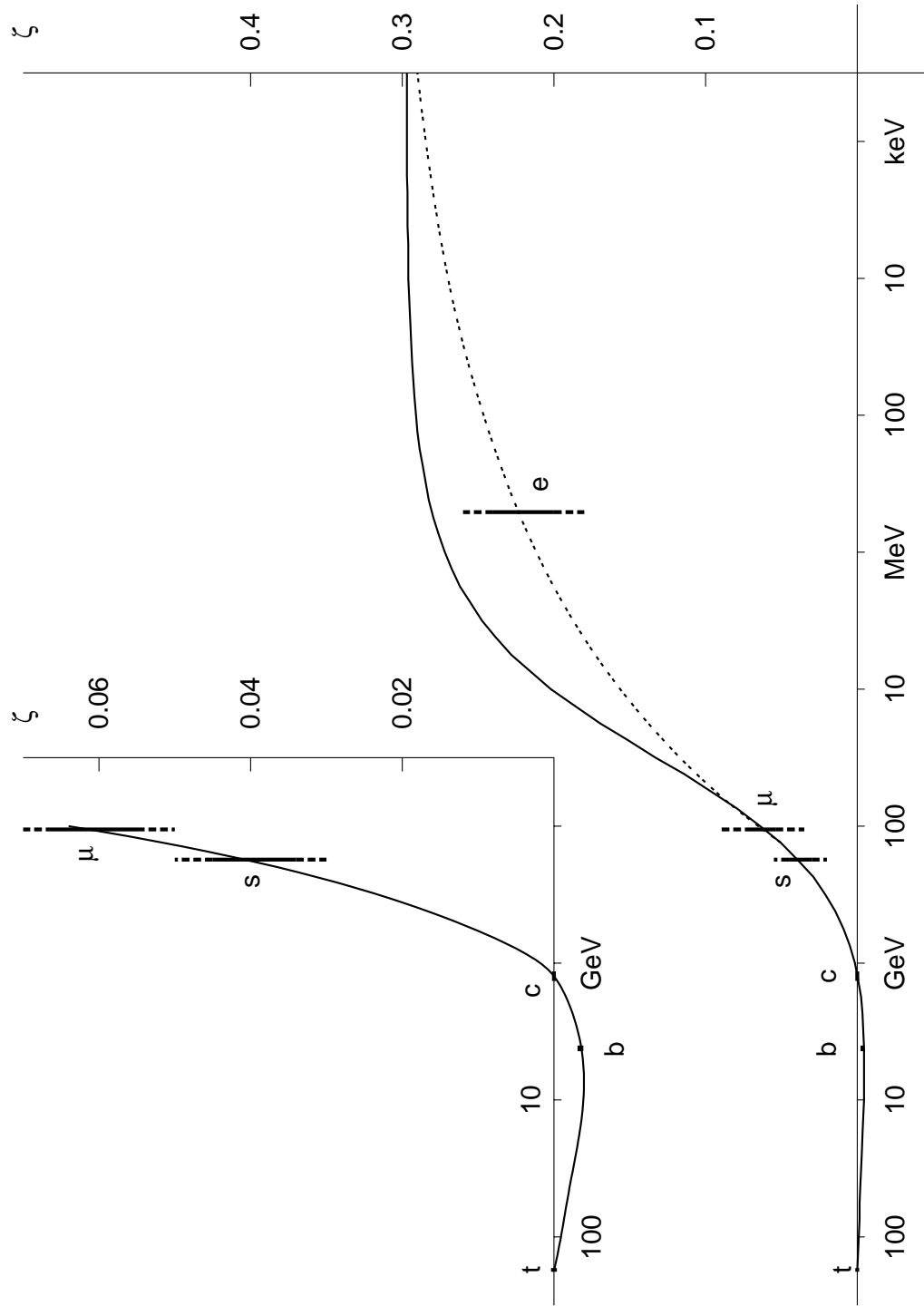


Figure 13: Projection of Figure 10 on to the $\mu\zeta$ -plane. The full curve represents the DSM one-loop calculation of [31] and the dashed curve its suggested deformation at low scales to fit the data on m_e and U_{e2} .

forms for the Higgs potential and Yukawa coupling possibly differing slightly from those at present assumed but yet achieving similar phenomenological success. If so, that would be ideal.

7 Other DSM Consequences

As seen above, the Dualized Standard Model has been quite successful in explaining fermion mass hierarchy and mixing, although one is not entirely certain as yet how much of the details in its structure is essential for this success. There is, however, still another angle to explore before one can properly gauge the significance of this seeming success. The DSM involves new assumptions beyond those already tested by experiment within the context of the conventional Standard Model, and is therefore bound to give some new physical predictions. One has thus to ask first, whether these new predictions agree with all existing experiment, and secondly, if they manage to survive these tests, whether they can be further tested by experiment in the near future.

One obvious direction to explore is flavour-violation which can occur in the DSM scheme in two ways. The first type is in common with all horizontal symmetry models in which the horizontal symmetry is mediated by bosons carrying the generation index. The exchange of such bosons would lead to flavour-changing neutral current (FCNC) effects, of which K meson decay to μe and $\mu - e$ conversion in nuclei are typical examples, as illustrated by the diagrams in Figure 14. The masses M_X of the mediating bosons are presumably high or otherwise they should have been seen already, and they are not. If so, then at the low energies where FCNC effects are studied in experiment, the reaction amplitudes would be suppressed by factors of order s/M_X^2 , leading to suppression in rates of order $(s/M_X^2)^2$. Hence, predicted rates of flavour-violations of this type can always be made sufficiently small to satisfy whatever experimental bounds by making M_X large, so long as no upper bound for M_X is prescribed by the theory. For this reason, for flavour-violating effects of this type, present bounds from experiment pose no imminent threat to the DSM scheme, nor indeed to any horizontal symmetry model.

Special to the DSM, however, is another type of flavour-violations which is potentially much more dangerous. One crucial property of the DSM explanation of fermion mass hierarchy and mixing is the rotation of the mass matrix with changing scales. And mass matrix rotation means that a mass

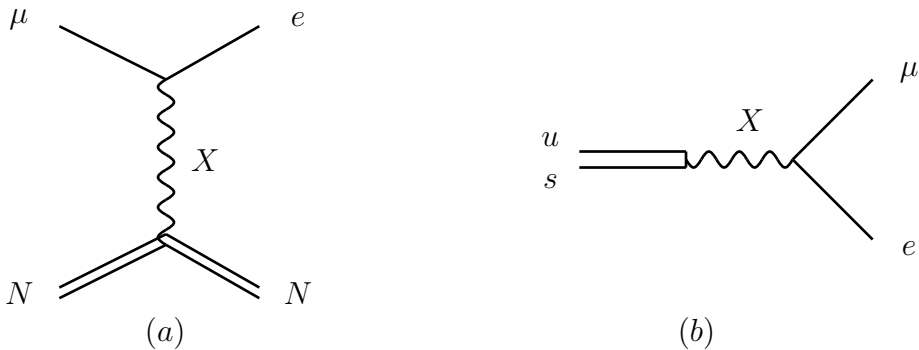


Figure 14: Diagrams representing schematically (a) $\mu-e$ conversion in nuclei, (b) $K_L \rightarrow \mu e$ decay, as FCNC effects via the exchange of heavy bosons X carrying generation index.

matrix diagonal at one scale will in general no longer be diagonal at another scale. For example, suppose we examine Compton scattering of a photon from an electron and the lepton mass matrix rotates as suggested in DSM. Then as detailed in section 4, the mass matrix is diagonal at the mass scales of the leptons, but not in general at other scales, and in particular not at the energy scale at which the Compton scattering experiment is performed. The reaction amplitude, which depends on the mass matrix, can thus be expected also not to be diagonal in the flavour states, hence leading to nonzero cross sections for the nondiagonal, flavour-violating reaction:

$$\gamma e \rightarrow \gamma \tau, \quad (7.1)$$

for example. In other words, purely kinematically, one could expect flavour-violation to result by virtue alone of the rotating mass matrix. And in a scheme such as DSM where the rotation speed, being tied to the fermion mass and mixing patterns and not adjustable to satisfy experimental bounds on flavour-violating reactions, the confrontation is potentially very dangerous.

This new type of flavour-violation due to a rotating mass matrix, to which we have given the name “transmutation” for easy reference, we have studied in some detail. It was found that, with the rotation speed constrained by the fermion mass and mixing pattern, transmutation effects from kinematics alone can be appreciable. For example, for the reaction:

$$e^+ e^- \longrightarrow \mu^+ \tau^-, \quad (7.2)$$

the integrated cross section estimated from a rotation speed read from, for example, Figure 9 or 10, is about 80 fb [43] at $\sqrt{s} = 10.85$ GeV, at which energy very high statistics is being collected by experiments such as BaBar [44] and Belle [45]. Although by itself this does not seem a large cross section, in view of the sensitivity of the above modern experiments with integrated luminosity of order 100 fb^{-1} , it is in fact frighteningly large, and should in principle be already detectable.

Fortunately for us, however, this estimate obtained from the kinematical effects alone of the rotating mass matrix is not yet the full prediction of the DSM scheme. In DSM, as detailed in section 3, the rotation of the fermion mass matrix arises from insertions in the fermion propagator. Thus, to study transmutation effects properly to 1-loop order, one will need to evaluate not just the 1-loop insertion in the fermion propagator but all diagrams to the same 1-loop order. For example, for the reactions (7.1) and (7.2), one will need to evaluate all the diagrams in respectively Figure 15 and 16 plus some others of no relevance to present considerations. This calculation has recently been done, and it was found that on summing all the relevant 1-loop diagrams, transmutation effects largely cancel leaving only terms of order s/M_X^2 in amplitude [29], with M_X being again the generic mass of the mediating bosons carrying generation index. In other words, the net effect of transmutation, i.e. flavour-violation due to mass matrix rotation, is just to give an additional contribution of the same order as flavour-changing neutral current effects.

In DSM this cancellation is not an accident but is based on quite general grounds. Explicitly, the calculation goes as follows. The relevant 1-loop insertion to the fermion propagator (3.20) can be rewritten in the form:

$$\Sigma(p) = -\frac{\delta m}{\rho^2} + \frac{1}{2}(\not{p} - m)B_L + \frac{1}{2}B_R(\not{p} - m) + \Sigma_c(p), \quad (7.3)$$

with

$$\begin{aligned} B_L &= -\frac{1}{16\pi^2} \sum_K \int_0^1 dx (1-x) \{ \bar{\gamma}_K^\dagger [\bar{C} - \ln(Q_0^2/\mu^2)] \bar{\gamma}_K \frac{1}{2} (1 + \gamma_5) \\ &\quad + \bar{\gamma}_K [\bar{C} - \ln(Q_0^2/\mu^2)] \bar{\gamma}_K^\dagger \frac{1}{2} (1 - \gamma_5) \}, \\ B_R &= -\frac{1}{16\pi^2} \sum_K \int_0^1 dx (1-x) \{ \bar{\gamma}_K [\bar{C} - \ln(Q_0^2/\mu^2)] \bar{\gamma}_K^\dagger \frac{1}{2} (1 + \gamma_5) \\ &\quad + \bar{\gamma}_K^\dagger [\bar{C} - \ln(Q_0^2/\mu^2)] \bar{\gamma}_K \frac{1}{2} (1 - \gamma_5) \}, \end{aligned} \quad (7.4)$$

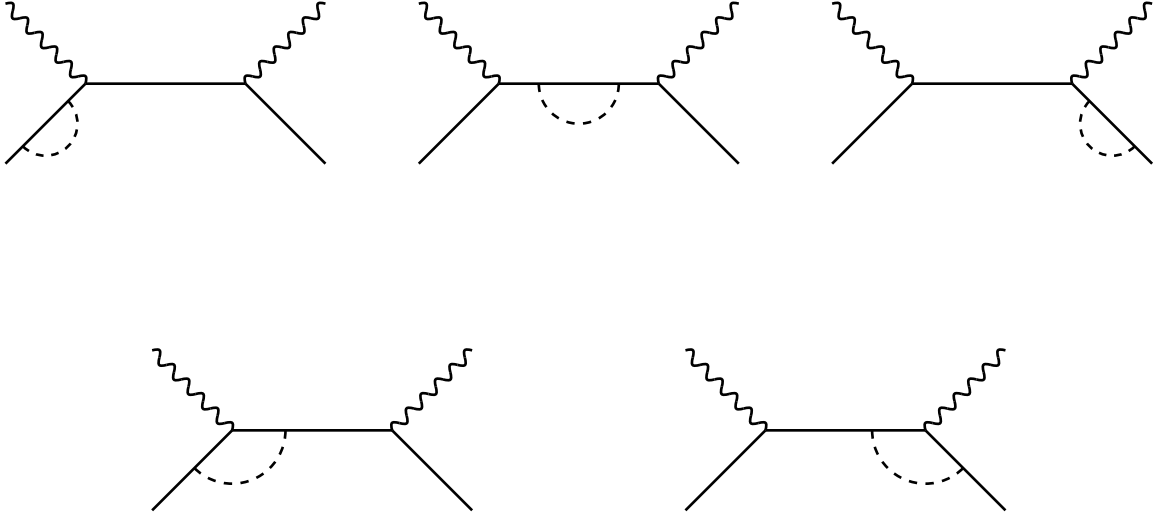


Figure 15: 1-loop diagrams contributing to transmutation in Compton scattering.

and $\Sigma_c(p)$ of a form which need not bother us here except to note that it is finite, independent of the renormalization scale, and of order s/M_K^2 , M_K being, one recalls, the mass of the dual colour Higgs boson appearing in the loop. The insertion of (7.3) to an internal fermion line thus gives:

$$\frac{1}{\not{p} - m} \longrightarrow \frac{1}{\not{p} - m'} - \frac{\rho^2}{2} B_L \frac{1}{\not{p} - m} - \frac{\rho^2}{2} \frac{1}{\not{p} - m} B_R - \rho^2 \frac{1}{\not{p} - m} \Sigma_c(p) \frac{1}{\not{p} - m} \quad (7.5)$$

and to an external fermion line:

$$u(p) \longrightarrow u'(p) - \frac{\rho^2}{2} B_L u(p) - \rho^2 \frac{1}{\not{p} - m} \Sigma_c(p) u(p) \quad (7.6)$$

$$\bar{u}(p) \longrightarrow \bar{u}'(p) - \frac{\rho^2}{2} \bar{u}(p) B_R - \rho^2 \bar{u}(p) \Sigma_c(p) \frac{1}{\not{p} - m} \quad (7.7)$$

where $u'(p)$ is a solution of the Dirac equation with the renormalized mass

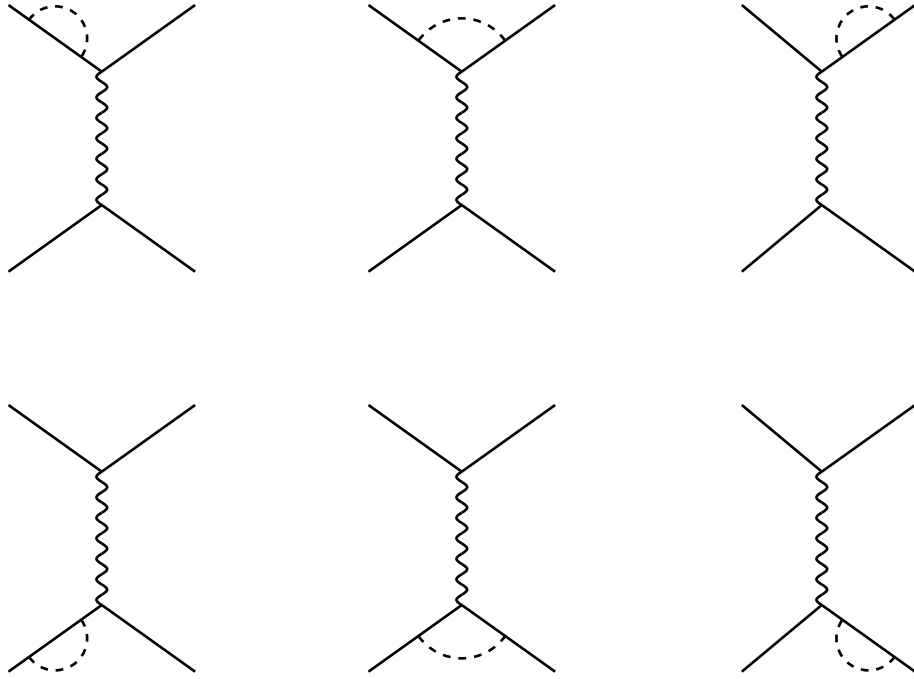


Figure 16: 1-loop diagrams contributing to transmutation in Bhabha scattering.

matrix m' :

$$(\not{p} - m')u'(p) = 0. \quad (7.8)$$

These conclusions follow closely those in e.g. ordinary QED apart from that, m being a matrix and therefore noncommuting, B_L and B_R are different.

A similar calculation gives as the vertex insertion:

$$\Lambda^\mu(p, p') = \frac{1}{2}\gamma^\mu L_L + \frac{1}{2}L_R\gamma^\mu + \Lambda_c^\mu(p, p'), \quad (7.9)$$

with

$$\begin{aligned} L_L = & -\frac{1}{16\pi^2} \sum_K \int_0^1 dx \int_0^x dy \{ \bar{\gamma}_K^\dagger [\bar{C} - \ln(P^2/\mu^2)] \bar{\gamma}_K \frac{1}{2} (1 + \gamma_5) \\ & + \bar{\gamma}_K [\bar{C} - \ln(P^2/\mu^2)] \bar{\gamma}_K^\dagger \frac{1}{2} (1 - \gamma_5) \}, \end{aligned}$$

$$\begin{aligned}
L_R &= -\frac{1}{16\pi^2} \sum_K \int_0^1 dx \int_0^x dy \{ \bar{\gamma}_K [\bar{C} - \ln(P^2/\mu^2)] \bar{\gamma}_K^\dagger \frac{1}{2} (1 + \gamma_5) \\
&\quad + \bar{\gamma}_K^\dagger [\bar{C} - \ln(P^2/\mu^2)] \bar{\gamma}_K \frac{1}{2} (1 - \gamma_5) \}, \tag{7.10}
\end{aligned}$$

where \bar{C} is the divergent constant in (3.21),

$$P^2 = m^2(1-y) + M_K^2 y - p^2 x(1-x) - p'^2(x-y)(1-x+y) + 2pp'(1-x)(x-y), \tag{7.11}$$

and $\Lambda_c^\mu(p, p')$ is finite, scale-independent and again of order s/M_K^2 .

One notices that L_L and L_R in (7.10) are very similar in form to respectively B_L and B_R in (7.4). Indeed, it can be shown that the pairs each differ only by terms of the order s/M_K^2 . This is not really surprising, being just a consequence of gauge invariance, and has a familiar parallel in ordinary electrodynamics.

With these results in hand, let us proceed now to calculate the amplitude for γe collision to 1-loop order. Adding to the tree diagrams the 1-loop diagrams of Figure 15, and making use of the results in (7.5), (7.7), and (7.9), one obtains the result:

$$\begin{aligned}
&\bar{u}'(p') \gamma^\mu \frac{i}{(\not{p} + \not{k}) - m'} \gamma_\mu u'(p) \\
&+ \frac{\rho^2}{2} \bar{u}(p') [\gamma^\mu (L_L - B_L) + (L_R - B_R) \gamma^\mu] \frac{i}{(\not{p} + \not{k}) - m} \gamma_\mu u(p) \\
&+ \frac{\rho^2}{2} \bar{u}(p') \gamma^\mu \frac{i}{(\not{p} + \not{k}) - m} [\gamma_\mu (L_L - B_L) + (L_R - B_R) \gamma_\mu] u(p), \tag{7.12}
\end{aligned}$$

plus only terms of order s/M_K^2 for large M_K . We recall further that in the differences $B_L - L_L$ and $B_R - L_R$, the divergent part and the scale dependence both cancel, leaving in each only a finite part which is again of order s/M_K^2 for large M_K . Hence, for large M_K the renormalized amplitude (7.12) will reduce simply to the first term there. And this first term has no nondiagonal elements since by definition, $u'(p')$ is a solution of the Dirac equation in (7.8) with mass m' and therefore an eigenvector of the renormalized mass matrix at any scale. In other words, transmutation cancels here to order s/M_K^2 as claimed. A similar analysis for e^+e^- leads to the same conclusion. Indeed, apart from some minor though nontrivial differences these results closely resemble familiar results in ordinary electrodynamics.

The above result that transmutation effects or flavour-violations due to mass matrix rotation cancel in DSM to order s/M_X^2 , M_X being the generic

mass scale of flavour-changing neutral bosons, is a great relief, since if they did not, they could easily lead to effects of such a size as to contradict experiment, if not immediately then in the very near future. And as explained above, such a contradiction cannot easily be avoided by readjusting parameters. As it is, the flavour-violating effects from mass matrix rotation is of the same order as flavour-changing neutral current (FCNC) effects and can thus be analysed together with the latter, to which we now turn.

Flavour-violation effects due to the direct exchange of flavour-changing neutral or generation index-carrying bosons have so far been analysed by us in DSM only for the gauge not the Higgs bosons, the reason being that the former are to us theoretically better understood. We believe, however, that the results obtained would be similar for both. The analysis follows closely the usual pattern for other horizontal symmetry models, with the predictions for flavour-violations strongly dependent on the exchanged boson mass. There is, however, one very important difference, namely that the DSM scheme, being strongly constrained by what has gone before will now be highly predictive. Indeed, once given an estimate of the exchanged gauge boson mass, then the DSM scheme so far developed will be able to give quite precise predictions for the rates or cross sections of most flavour-violation effects. The reason is that if one accepts the tenets of the DSM scheme, then both the coupling strength of the gauge boson and its branching into various modes will be given. The first will be given by the Dirac quantization condition (2.13) relating the required coupling \tilde{g} of dual colour to the well-known coupling of ordinary colour g , while the second will be given by the orientations of the state vectors of the various fermion states relative both to one another and to the gauge bosons, and these orientations are already determined by the calculation in section 5 of the rotating mass matrix. For a first estimate of FCNC effects of relevance to the present experimental situation, only the 1-boson exchange diagrams need be calculated, higher order diagrams being suppressed by the high boson mass. And these 1-boson exchange diagrams are calculable once given the gauge boson mass and the couplings to fermions. Hence, apart from some technical details connected with the soft hadronic, nuclear or atomic physics inherent in respectively, for example, hadron decays, $\mu - e$ conversion in nuclei, and muonium conversion, which can be handled by almost standard methods, the calculations are relatively familiar and straightforward. We need therefore only quote here some of the results as examples.

From an analysis of meson FCNC decays and mass splittings, one finds that the strongest present bound on the flavour-violating gauge boson mass

M_X comes from $K_L - K_S$ mass splitting which gives a lower bound on the boson mass of order $M_X/\tilde{g} \sim 400$ TeV. Taking this estimate as benchmark value, and using the couplings to various channels deduced in the DSM scheme, one can then calculate the branching ratios for various FCNC meson decays, some of the most interesting examples of which are listed in Table 1 [30]. Further, applying the same considerations to coherent $\mu - e$ conversions in nuclei with the same benchmark value for the gauge boson mass, one obtains the conversion rates for some experimentally interesting nuclei as shown in Table 2 [46]. One notices first that the predictions listed in both tables are quite detailed and precise for reasons already explained, and secondly, that several of these are already close to the present experimental limits. This means that if any one of these FCNC effects is found in experiment, hence giving an actual value for the gauge boson mass rather than just a lower limit, then the correlated bounds listed in the 2 tables can be used to give absolute predictions for all the others. Or else, if some other means is available to suggest a value for the gauge boson mass, the same predictions can also be obtained.

Does there then exist any means for estimating the flavour-changing neutral boson mass without first observing flavour-violation? There is perhaps one way which takes us interestingly to an entirely different area of physics and another potentially dangerous prediction of the DSM scheme. This arises as follows. The exchange of flavour-changing gauge bosons which leads to flavour-violations is suppressed at low energies by the large value of the boson mass to order s/M_X^2 in amplitude, which is the normal reason given for FCNC effects being so small, and hence not yet observed. This is a copy of the explanation why “weak” interaction were considered weak in the old days before the W and Z bosons were discovered although the couplings of these bosons, as we now know, are by no means so very small. Indeed, it is by now a familiar fact that when experimental energies rise beyond the W and Z mass, weak interaction cross sections become sizeable. In the same manner, therefore, for the processes mediated by the even heavier flavour-changing bosons, cross sections will become large also when energy is as large as the boson mass. In fact, if one believes DSM, then the effective interaction will become very strong given that the boson coupling is constrained by the Dirac quantization condition (2.13) to be of order $\tilde{g} \sim 10$. This means that any particle carrying the generation index which allows it to couple to the flavour-changing bosons and hence interact by exchanging them will acquire very strong interactions at high energies of order $\sqrt{s} \sim M_X$. In particular, even neutrinos which are believed now to exist in generations are expected

	Theory	Experiment
$\text{Br}(K^+ \rightarrow \pi^+ e^+ e^-)$	4×10^{-15}	2.9×10^{-7}
$\text{Br}(K^+ \rightarrow \pi^+ \mu^+ \mu^-)$	2×10^{-15}	7.6×10^{-8}
$\text{Br}(K^+ \rightarrow \pi^+ e^+ \mu^-)$	2×10^{-15}	7×10^{-9}
$\text{Br}(K^+ \rightarrow \pi^+ e^- \mu^+)$	2×10^{-15}	2.1×10^{-10}
$\text{Br}(K^+ \rightarrow \pi^+ \nu \bar{\nu})$	2×10^{-14}	1.5×10^{-10}
$\text{Br}(K_L \rightarrow e^+ e^-)$	2×10^{-13}	9×10^{-12}
$\text{Br}(K_L \rightarrow \mu^+ \mu^-)$	7×10^{-14}	7.2×10^{-9}
$\text{Br}(K_L \rightarrow e^\pm \mu^\mp)$	1×10^{-13}	4.7×10^{-12}
$\text{Br}(K_S \rightarrow \mu^+ \mu^-)$	1×10^{-16}	3.2×10^{-7}
$\text{Br}(K_S \rightarrow e^+ e^-)$	3×10^{-16}	1.4×10^{-7}

Table 1: Branching ratios for rare leptonic and semileptonic K decays. The first column shows the DSM predictions from one-dual gauge boson exchange with the boson mass scale at a benchmark value of 400 TeV. The second column gives either the present experimental limits on that process if not yet observed or the actual measured value for that process. In the latter case, it means that the process can go by other mechanisms such as second-order weak so that our predictions with dual gauge boson exchange will appear as corrections to these. All the empirical entries are from the data booklet [1].

Element	$B_{\mu-e}^{\text{theor.}}$	$B_{\mu-e}^{\text{exp. lim.}}$
$^{27}\text{Al}_{13}$	1.4×10^{-12}	n.a.
$^{32}\text{S}_{16}$	1.9×10^{-12}	7×10^{-11}
$^{48}\text{Ti}_{22}$	2.3×10^{-12}	4.3×10^{-12}
$^{207}\text{Pb}_{82}$	2.7×10^{-12}	4.6×10^{-12}

Table 2: Theoretical estimates for the ratio of the $\mu - e$ conversion rate to the μ capture rate compared with present experimental limits. These values are calculated with the dual gauge boson mass scale taken at the benchmark value of 400 TeV.

also to acquire this new interaction at high energy.

This last is an astounding and at first sight very dangerous prediction, for as we very well know, there is no indication at all in present day experiment of such a phenomenon. Indeed, we were very worried at first until we realized that the gauge boson mass is constrained by present bounds on FCNC effects, as explained above, to be larger than around 400 TeV, which is an enormous energy not achievable in the laboratory either today or in the near future. The only chance for observing effects at such energy would be in cosmic rays, and even there the event rate would be very, very small. For a cosmic ray particle hitting a nucleon in the atmosphere, $\sqrt{s} \sim 400$ TeV corresponds to a primary energy of about 10^{20} eV. Cosmic ray events at such primary energies are known only in extensive air showers and even there are very rare, incident on earth at an estimated rate of only about 1 event per square kilometer per century. Though rare, however, they have caught particular attention, for ever since their observation in experiment they have been a theoretical headache, for the following reason.

Although the origin of cosmic rays is still largely unknown so that primary energies in excess of 10^{20} eV are in principle possible, there is a bound, known as the GZK cut-off, on the energy of particles arriving on earth from a distance of greater than about 50 Mpc. Indeed, it was shown by Greisen and by Zatsepin and Kuz'min [47] already in 1966 that a proton or nucleus with such primary energies would quickly degrade in energy by interacting with the 2.7 K microwave background via the following reaction:

$$p(N) + \gamma \longrightarrow p(N) + \pi, \quad (7.13)$$

and hence not arrive on earth with their primary energies intact, if they come from a distance of over 50 Mpc. Yet, over the years some 10 such events are claimed to have been seen, and they are beautiful things developing into a shower [48] with as many as 10^{11} charged particles!

So what are they? According to Greisen, Zatsepin and Kuz'min, they cannot be protons or nuclei coming from more than 50 Mpc away. They are probably also not from a nearby source, for within a radius of 50 Mpc, there are no known astrophysical sources capable of producing particles with such high energies. Likewise, they are thought not to be photons, which can also interact with the microwave background by pair production and hence cannot maintain their high energy over long distances. And they cannot be neutrinos which can survive the journey but, having only weak interactions, cannot produce air showers. That is, unless neutrinos can acquire strong interactions at these ultra high energies as predicted above by the DSM.

What would happen if one accepts that neutrinos do become strongly interacting for $\sqrt{s} \gtrsim 400$ TeV as the DSM suggests? Then any source such as an active galactic nucleus which is capable of producing protons of such energies will also be able to produce neutrinos at these energies just by proton collisions via the said strong interactions. Once produced, the neutrinos will be able to escape from the active galactic nucleus, although protons cannot because of the strong magnetic fields surrounding the source. Further, the neutrinos will be able to survive the long journey through the microwave background in contrast to protons which cannot do so because of the GZK reaction (7.13). And when the neutrinos arrive on earth, they will interact strongly by hypothesis with the air nuclei to produce the extensive air showers seen. Thus the hypothesis seems neatly to have passed all the initial tests and qualifies as a viable candidate solution to the GZK problem. In addition, it has even an explanation for a possible effect of these air showers reported by one experiment [50]. Out of the dozen or so events claimed to have been seen by this group, there are 3 doublets and 1 triplet observed, the members of each multiplet being collimated within the experimental angular resolution of 1–2 degrees. This suggests that members of each multiplet originate from the same source. However, if the primaries were protons or nuclei, even when they originated from the same source, with in general different energies they would have been deflected differently by the intergalactic magnetic fields and lost their common direction. Neutrinos, on the other hand, being neutral, would not be deflected by the magnetic fields and would remain collimated if they originate from the same source.

Interestingly, the above suggestion of post-GZK air showers being due to neutrinos acquiring strong interactions at high energy can be subjected to further experimental tests. First of all, the hypothesis being that neutrinos interact strongly only at energies above the flavour-changing boson mass, it follows that the GZK threshold itself would put an upper bound on that mass. Harking back then to our earlier discussion of FCNC effects, this is exactly what is needed to constrain the magnitude of these effects. As it happens, the upper bound on the boson mass obtained from the GZK threshold, as seen above, is close to the lower bound obtained before from $K_L - K_S$ mass splitting. One would then obtain an actual estimate of the boson mass and could thus convert the previous bounds shown in e.g. Tables 1 and 2 into actual predictions. Although this estimate for the boson mass is very crude since all effects involved depend on the mass raised to the 4th power, nevertheless, it suggests in Tables 1 and 2 that FCNC effects may be just around the corner for experimental observation, and that these predictions

can soon be tested. Secondly, in cosmic ray physics proper, the hypothesis also suggests that air showers above the GZK cut-off should occur at lower heights in the atmosphere than those below the cut-off. The argument goes as follows. The average height of air showers depend on the penetrating power of the incoming primary particle which in turn depends on the particle's cross section with air nuclei. Now according to our hypothesis, pre-GZK showers are from protons or nuclei and post-GZK showers from neutrinos, and since protons and neutrinos presumably have different cross section with air nuclei, they should occur at different average heights. In Figure 17 is shown the change in average heights across the GZK threshold assuming different ratios of neutrino/proton cross sections with air nuclei. In particular, if one assumes that the neutrino still appears as a point to the air nucleus at high energy, then the substitution of the known proton and air nucleus radii into a geometric picture gives an estimate for the ratio between neutrino and proton cross sections of $\sigma_{\nu A}/\sigma_{pA} \sim 1/2$, corresponding to a change in height as shown in Figure 17 which is sizeable. Such an effect may thus be looked for in Auger [51] or other future experiments.

Despite the scarcity and still somewhat tenuous nature of the data on post-GZK air showers, we have described the DSM picture for them at some length, first for the sheer beauty of these events and our own fascination with them, and secondly for the special role that they may play as a test for the DSM scheme. As we have noted above already, despite the many tests to which the DSM predictions have been subjected and so far survived, not a single one hangs crucially upon the hypothesis that the horizontal symmetry of fermion generations is indeed identical to dual colour as suggested, apart from this one on post-GZK air showers. There was an important point in the above discussion that we have so far deliberately glossed over, namely that even given that neutrinos do acquire a strong interaction at extreme energies, it still does not mean that they will necessarily give air showers on collision with air nuclei, for which is needed not just a strong interaction between the neutrino and the air nucleus but a large hadronic-sized cross section. An interaction between the neutrino with the quarks inside the air nucleus which is short-ranged, as would happen if the horizontal symmetry has nothing to do with colour, say of the order of the mass M_X of the heavy boson exchanged, will still give only minuscule cross sections no matter how strong it is. However, it was argued in [52] that if the generation symmetry is indeed identical to dual colour, then the neutrino at extreme energy will interact not only strongly but coherently with the air nuclei, hence giving hadronic sized cross sections sufficient to produce air showers in the atmosphere. Indeed,

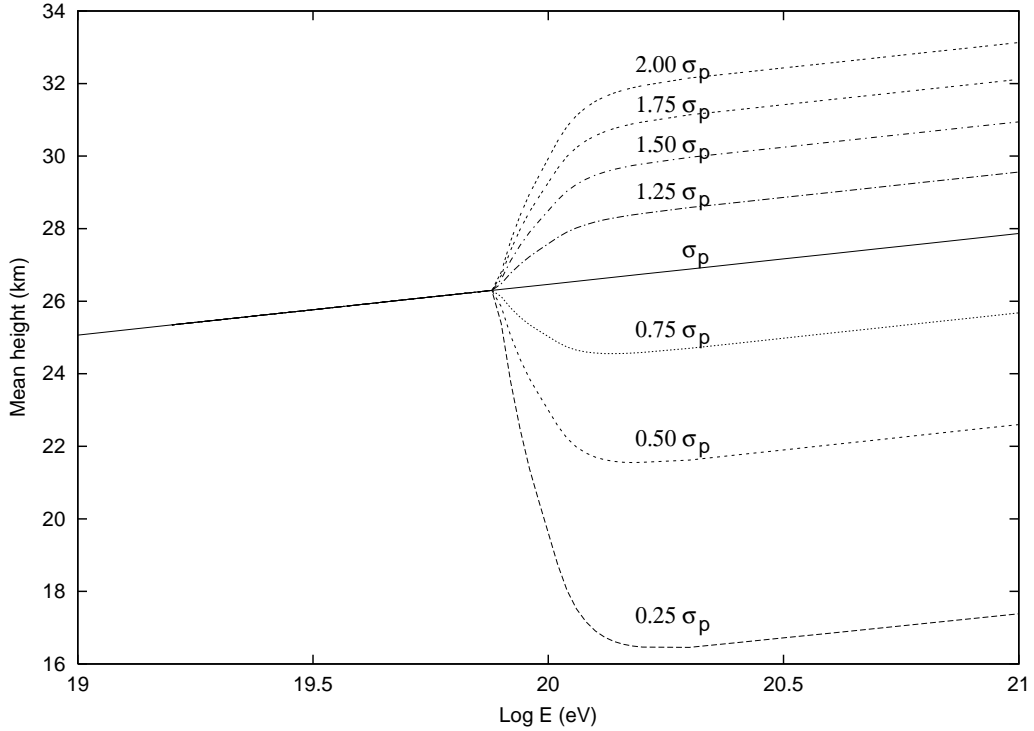


Figure 17: Average equivalent vertical height of air showers as a function of the primary energy across the GZK cut-off assuming post-GZK primaries of varying cross sections.

this consideration is implicit in the geometric picture invoked above to infer a νA cross section of about a half of that of pA . Although the argument given there is only qualitative, it is an important point to bear in mind in considering the above explanation of post-GZK air showers as initiated by strongly interacting neutrinos.

In summary, as far as flavour-violation and related questions are concerned, which are the primary worry for the rotating mass matrix forming the basis of the DSM's main results on fermion mass and mixing patterns, the scheme seems to have survived all tests so far performed, and in the case of cosmic ray air showers it seems even to have offered a new explanation for an old puzzle. However, the job of surviving tests and limits is never done and can be prolonged ad infinitum until one runs out of ideas or breath or

both. We have performed more tests, which include for example an obvious one on neutrinoless double-beta decay [53], and which DSM also survives.

8 Remarks

In conclusion, it would seem that the DSM scheme has so far largely succeeded in what it sets out to achieve, namely to suggest a *raison d'être* for 3 fermion generations and to explain their unusual mass and mixing patterns. Apart from CP-violation, even near quantitative results have been obtained already with the 1-loop calculations performed in the energy region where it is expected to be valid. And in all areas explored up to now where potential difficulties could arise, no violation of existing experimental bounds is found.

There is, however, still one feature in the present formulation of the scheme which leaves something to be desired. The construction of the scheme as set out, for example, in Section 3, seems to come in 2 parts, first the theoretical idea of deriving the generation symmetry and its breaking from duality, and second, the construction of a phenomenological model in terms of a Higgs potential and a Yukawa coupling, which though suggested by, cannot claim to follow from, the initial duality concepts. And although duality does lead directly to the prediction of 3 and only 3 generations, the rest of the result on mixing and so on are consequences of the phenomenological model with at present but tenuous links to duality. Granted that even when considered as a purely phenomenological model, the derivation by itself of these latter results seems already not a mean achievement, one is nevertheless still some way from being able to claim that the origin of generations as dual colour is now understood.

It seems to us, therefore, that to advance further, one should perhaps proceed in 2 directions. First, one should seek testable predictions of the scheme which depend directly on the hypothesis that dual colour is generation symmetry, of which we mentioned a possible example with post-GZK air showers. Secondly, one should try to derive directly from duality and related concepts either the above phenomenological model itself or else a scheme close to it which is capable of giving the same results. This is an ideal to strive for, but whether it can be achieved we do not know.

Acknowledgement

Much of the original work which has gone into the above review, as well as the manner in which it is presented, has been achieved with the constant, close and always thoroughly enjoyable collaboration of José Bordes, who only escapes being a co-author by the circumstantial accident of not being physically present at the Zakopane Summer School.

References

- [1] Particle Physics Booklet, (2000), D.E.Groom et al., extracted from the Review of Particle Physics, Euro. Phys. Journ. C15, (2000) 1.
- [2] N. Cabibbo, Phys. Rev. Lett. 10, 531 (1963).
- [3] M. Kobayashi and T. Maskawa, Prog. Theor. Phys. 49, 652 (1973).
- [4] Z. Maki, M. Nakagawa and S. Sakata, Prog. Theor. Phys. 28, 870 (1962).
- [5] Superkamiokande data, see e.g. talk by T. Toshito at ICHEP'00, Osaka (2000).
- [6] Soudan II data, see e.g. talk by G. Pearce, at ICHEP'00, Osaka (2000).
- [7] Q.R. Ahmad et al. Phys. Rev. Lett. 87, 071307, (2001), nucl-ex/0106015.
- [8] B.T. Cleveland et al., Astropart. Phys. 496 (1998) 505.
- [9] J. Abdurashitov et al., Phys. Rev. C60 (1999) 055801.
- [10] J.W. Hampel et al., Phys. Lett. B447 (1999) 127.
- [11] CHOOZ collaboration, M. Apollonio et al., Phys. Lett. B420, 397, (1998), hep-ex/9711002.
- [12] L. Wolfenstein, Phys. Rev. D17, 2369, (1978); S.P. Mikheyev and A.Yu. Smirnov, Nuovo Cim. 9C, 17 (1986).
- [13] P.A.M. Dirac, Proc. Roy. Soc. London, A133, 60, (1931).
- [14] Chan Hong-Mo and Tsou Sheung Tsun, *Some Elementary Gauge Theory Concepts*, World Scientific, Singapore, 1993.

- [15] Chan Hong-Mo and Tsou Sheung Tsun, Phys. Rev. D56, 3646 (1997), hep-th/9702117.
- [16] Tai Tsun Wu and Chen Ning Yang, Phys. Rev. D14, 437 (1976).
- [17] Chan Hong-Mo, Peter Scharbach and Tsou Sheung Tsun, Ann. Phys. (NY) 167, 454 (1986).
- [18] C.H. Gu and C.N. Yang, Sci. Sin. 28, 483 (1975).
- [19] A.M. Polyakov, Nucl. Phys. 164, 171 (1980).
- [20] Chan Hong-Mo, Peter Scharbach and Tsou Sheung Tsun, Ann. Phys. (NY) 166, 396 (1986); Chan Hong-Mo and Tsou Sheung Tsun, Acta Phys. Pol. B17, 259, (1986).
- [21] Chan Hong-Mo, Jacqueline Faridani, and Tsou Sheung Tsun, Phys. Rev. D53, 7293 (1996), hep-th/9512173.
- [22] The idea of a possible “horizontal symmetry” linking generations is quite old. Examples of some early references are: F. Wilczek and A. Zee, Phys. Rev. Lett. 42, 421, (1979); A. Davidson and K.C. Wali, Phys. Rev. D20, 1195, (1979), D21, 787, (1980); T. Maehara and T. Tanagida, Prog. Theor. Phys. 61, 1434, (1979); T. Yanagida, Phys. Rev. D22, 1826, (1980).
- [23] G. 't Hooft, Nucl. Phys. B138, 1 (1978); Acta Physica Austriaca Suppl. XXII, 531 (1980).
- [24] Chan Hong-Mo, Jacqueline Faridani, and Tsou Sheung Tsun, Phys. Rev. D52, 6134 (1995).
- [25] See, e.g., F.W. Heyl et al., Rev. Mod. Phys. 48, 393, (1976).
- [26] Chan Hong-Mo and Tsou Sheung Tsun, Phys. Rev. D57, 2507, (1998), hep-th/9701120.
- [27] Steven Weinberg, Phys. Rev. D7, 2887, (1973).
- [28] José Bordes, Chan Hong-Mo, Jacqueline Faridani, Jakov Pfaudler, and Tsou Sheung Tsun, Phys. Rev. D58, 013004, (1998), hep-ph/9712276.
- [29] José Bordes, Chan Hong-Mo and Tsou Sheung Tsun, Phys. Rev. D65, 093006, (2002), hep-ph/0111369.

- [30] José Bordes, Chan Hong-Mo, Jacqueline Faridani, Jakov Pfaudler, and Tsou Sheung Tsun, Phys. Rev. D60, 013005, (1999), hep-ph/9807277.
- [31] José Bordes, Chan Hong-Mo and Tsou Sheung Tsun, Eur. Phys. J. C. 10, 63 (1999), hep-ph/9901440.
- [32] José Bordes, Chan Hong-Mo and Tsou Sheung Tsun, hep-ph/0302199.
- [33] H. Arason, D.J. Castaño, B. Kesthelyi, S. Mikaelian, E.J. Piard, P. Ramond, and B.D. Wright, Phys. Rev. D46, 3945, (1992).
- [34] C. Jarlskog, in *CP Violation*, ed. C. Jarlskog, World Scientific, Singapore, 1989.
- [35] See e.g. L.P. Eisenhart, *A Treatise on the Differential Geometry of Curves and Surfaces*, Ginn and Company 1909, Boston; M.P. do Carmo, *Differential Geometry of Curves and Surfaces*, Prentice-Hall 1976, Englewood Cliffs, New Jersey.
- [36] José Bordes, Chan Hong-Mo, Jakov Pfaudler, and Tsou Sheung Tsun, Phys. Rev. D58, 053006, (1998), hep-ph/9802436.
- [37] M. Gell-Mann, P. Ramond, and S. Slansky in *Supersymmetry*, ed. F. van Nieuwenhuizen and D. Freeman (North Holland, Amsterdam, 1979); T. Tanagida, Prog. Theor. Phys., B135, 66, (1978).
- [38] José Bordes, Chan Hong-Mo, Jakov Pfaudler, and Tsou Sheung Tsun, Phys. Rev. D58, 053003, (1998), hep-ph/9802420.
- [39] R. M. Barnett et. al, Phys. Rev. D54, 1 (1996).
- [40] T. Appelqvist and J. Carrazzone, Phys. Rev. D11 (1975) 2865.
- [41] José Bordes, Chan Hong-Mo and Tsou Sheung Tsun, hep-ph/0203124, to appear in Eur. Phys. J. C.
- [42] S.H. Ahm et al., Phys. Lett. B511, 178, (2001), hep-ex/0103001.
- [43] José Bordes, Chan Hong-Mo and Tsou Sheung Tsun, hep-ph/0111175.
- [44] BaBar collaboration, see e.g. D.G. Hitlin, talk given at the 30th International Conference on High energy Physics, Osaka, Japan, Jul.-Aug. 2000, hep-ex/0011024.

- [45] Belle Collaboration, see e.g. paper presented at the 7th International Conference on B Physics at Hadronic Machines, Kibutz Maagan, Israel, Sep. 2000, hep-ex/0101033.
- [46] José Bordes, Chan Hong-Mo, Ricardo Gallego, and Tsou Sheung Tsun, Phys. Rev. D61, 00077702, (2000), hep-ph/9909321.
- [47] K. Greisen, Phys. Rev. Letters, 16 (1966) 748; G.T. Zatsepin and V.A. Kuz'min, JETP Letters, 4 (1966) 78.
- [48] See e.g. M. Boratov, in Proc. 7th International Workshop on Neutrino Telescopes, Venice (1996), astro-ph/9605087.
- [49] See e.g. M. Takeda et al., Phys. Rev. Letters, 81, 1163, (1998) and references therein.
- [50] M. Takeda et al., Astrophys. Journ. 522 (1999) 225; N. Hayashida et al., astro-ph/0008102.
- [51] The Pierre Auger Observatory Design Report (2nd ed.), 14 March 1997.
- [52] J. Bordes, Chan Hong-Mo, J. Faridani, J. Pfaudler, and Tsou Sheung Tsun, Astroparticle Phys. 8, 135, (1998), astro-ph/9707031; see also hep-ph/9705463, (1997) unpublished; hep-ph/9711438, published in the *Proceedings of the International Workshop on Physics Beyond the Standard Model: from Theory to Experiment*, (ed. I Antoniadis, LE Ibañez and JWF Valle) Valencia, October 1998, World Scientific (Singapore) 1998; José Bordes, Chan Hong-Mo and Tsou Sheung Tsun, astro-ph/0012384.
- [53] José Bordes, Chan Hong-Mo, Ricardo Gallego, and Tsou Sheung Tsun, Phys. Rev. D63, 117701, (2001), hep-ph/0012242.